FOSSIL ENERGY

DOE/BC/14953-20
(DE98000481)

INCREASED OIL PRODUCTION AND RESERVES FROM IMPROVED COMPLETION TECHNIQUES IN THE BLUEBELL FIELD, UINTA BASIN, UTAH

Annual
October 1, 1996 - September 30, 1997

By
Milind D. Deo
Craig D. Morgan

May 1998

Performed Under Contract No. DE-FC22-92BC14953

Utah Geological Survey
Salt Lake City, Utah

National Petroleum Technology Office
U. S. DEPARTMENT OF ENERGY
Tulsa, Oklahoma

Increased Oil Production And Reserves From Improved Completion Techniques In The Bluebell Field, Uinta Basin, Utah

Annual Report
October 1, 1996 to September 30, 1997

By
Milind D. Deo
Department of Fuels and Chemical Engineering
University of Utah
and
Craig D. Morgan
Utah Geological Survey

April 1998

Work Performed Under Contract No. DE-FC22-92BC14953

Prepared for
U.S. Department of Energy
Assistant Secretary for Fossil Energy

Gary D. Walker, Project Manager
National Petroleum Technology Office
P.O. Box 3628
Tulsa, OK 74101

Submitted by:
Utah Geological Survey
Box 146100
Salt Lake City, UT 84114-6100

US/DOE Patent Clearance is not required prior to the publication of this document

CONTENTS

ABSTRACT 1

EXECUTIVE SUMMARY 3

1. INTRODUCTION 5
    1.1. Project Status 5
    1.2. Geology and Field Background 5

2. HORIZONTAL AND VERTICAL DISTRIBUTION OF POROSITY AND OIL PRODUCTION 8
    2.1. Introduction 8
    2.2. Horizontal and Vertical Distribution of Non-Fractured Porosity 8
    2.3. Horizontal and Vertical Distribution of Oil Production 8
    2.4. Summary and Conclusions 9

3. CHARACTERIZATION OF FRACTURE PROPERTIES 14
    3.1. Introduction 14
    3.2. Background: Fracture Characterization Methods 14
    3.3. Markov-Bayes Method 14
    3.4. Procedure for Markov-Bayes Simulations 16
    3.5. The Data Set 17
    3.6. Three Different Approaches Used 18
    3.7. Comparison of Fracture Frequencies Determined by Using the Three Approaches 18
    3.8. Generation of Porosity and Permeability Distributions 19
    3.9. Reservoir Flow Simulations 19
    3.10. Summary and Conclusions 20

4. DEVELOPMENT OF A PARALLEL FRACTURED RESERVOIR SIMULATOR 31
    4.1. Introduction 31
    4.2. Parallel Computation and Reservoir Simulation 31
    4.3. The Message Passing Interface – MPI Standard 31
    4.4. The Fractured Reservoir Model 32
    4.5. Development of the Parallel Version of the Fractured Model 32
    4.6. Development of Parallel Program 35
        4.6.1. Initialization 35
        4.6.2. Read and Assign Input Parameters 35
        4.6.3. Formulate Fracture and Matrix Pressure Equations 36
        4.6.4. Solve Local Fracture and Matrix Flow Equations 36
        4.6.5. Calculation of Saturation Values 37
        4.6.6. Continue to the Next Step 37
    4.7. Performance of the Parallel Program on a Shared Memory Machine 37

4.8. Summary and Conclusions 38

5. RECOMPLETION OF THE MICHELLE UTE 7-1 WELL 54
5.1. Introduction 54
5.2. Cased-Hole Log Interpretation of the Michelle Ute Well 54
5.3. Acid Treatment of the Michelle Ute Well 56
5.4. Oil Production Before and After Stimulation 57
5.5. Summary and Conclusions 57

6. TECHNOLOGY TRANSFER 62
6.1. Introduction 62
6.2. Information Exhibits 62
6.3. Publications 62
6.4. Petroleum News 62
6.5. Internet 62

REFERENCES 64

ILLUSTRATIONS

Figure 1.1. Location of Bluebell field, Duchesne and Uintah Counties, Utah. 7
Figure 2.1. Map of the Bluebell field showing the location of wells used for the porosity-times-feet bar graphs cross sections in Fig. 2.3. 10
Figure 2.2. Bar graphs showing porosity-times-feet per 200-ft drill-depth interval from wells in the Bluebell field. 11
Figure 2.3. Map of the Bluebell field showing the wells used for the vertical-distribution-of-oil-production bar graphs cross sections in Fig. 2.5. 12
Figure 2.4. Bar graphs showing the vertical distribution of the oil production from wells in the Bluebell field based on temperterature and spinner logs 13
Figure 3.1. A scattergram and corresponding prior probability distribution function. 23
Figure 3.2. A schematic diagram showing steps involved during the Markov-Bayes simulation procedure. 24
Figure 3.3. A map of the Bluebell field showing locations of the core samples. 25
Figure 3.4. Cross section showing the formations and depths of core samples. 26
Figure 3.5. Fracture frequency distribution in different rock types. 27
Figure 3.6. Comparisons of probability distribution functions for different fracture frequency categories for shale. 28
Figure 3.7. Comparisons of probability distribution functions for different fracture frequency categories for sandstone. 29
Figure 3.8. Oil production comparisons for the reservoir models developed with fracture frequency distributions generated through three different approaches. 30
Figure 4.1. Conceptual diagram showing the approach taken to solve the pressure equations. 39

Figure 4.2. An example two dimensional computational grid distributed over a number of processors. 40
Figure 4.3. Communications involved during Gauss-Seidel relaxation. 41
Figure 4.4. An example tridiagonal matrix splitting as a result of domain decomposition. 42
Figure 4.5. Matrix splitting for iterative tridiagonal solution method. 43
Figure 4.6. Basic steps involved in parallel flow simulations 44
Figure 4.7. Comparison of computational time for the calculation of coefficient matrices for the serial program (1 processor) and parallel program (2 and 4 processors) on SGI Power Challenge. 50
Figure 4.8. Comparison of computational times for solution of fracture pressure equation on the SGI Power Challenge. 51
Figure 4.9. Comparison of computation times for the solution of matrix pressure equation on the SGI Power Challenge. 52
Figure 4.10. Comparison of total computation time for one time step of the simulation on the SGI Power Challenge. 53
Figure 5.1. Cased-hole logs (13,400-13,900 ft [4,073.6-4,225.6 m]) of a portion of the Flagstaff Member of the Green River Formation in the Michelle Ute 7-1 well 58
Figure 5.2. Cased-hole logs (12,900-13,400 ft [3,921.6-4,073.6 m]) of a portion of the Flagstaff Member of the Green River Formation in the Michelle Ute 7-1 well 58
Figure 5.3. Daily oil production from the Michelle Ute 7-1 well 61

TABLES

Table 3.1. Comparison of proportions of fracture frequency categories with sample data for three approaches. 21
Table 3.2. Porosity and permeability data set. 21
Table 3.3. Comparison of cdfs for one output realization with sample data. 22
Table 5.1. Additives used in the stimulation of the Michelle Ute 7-1 well. 56

ABSTRACT

The Bluebell field is productive from the Tertiary lower Green River and Colton (Wasatch) Formations of the Uinta Basin, Utah. The productive interval consists of thousands of feet of interbedded fractured clastic and carbonate beds deposited in the ancestral Lake Uinta. Wells in the Bluebell field are typically completed by perforating 40 or more beds over 1000 to 3000 vertical ft (300-900 m), then stimulating the entire interval with hydrochloric acid. This technique is often referred to as the “shot gun” completion. Completion techniques used in the Bluebell field were discussed in detail in the Second Annual Report (Curtice, 1996). The shot-gun technique is believed to leave many potentially productive beds damaged and/or untreated, while allowing water-bearing and low-pressure (thief) zones to communicate with the wellbore.

A two-year characterization study involved detailed examination of outcrop, core, well logs, surface and subsurface fractures, produced oil-field waters, engineering parameters of the two demonstration wells, and analysis of past completion techniques and effectiveness. The study was intended to improve the geologic characterization of the producing formations and thereby develop completion techniques specific to the producing beds or facies instead of a shot gun approach to stimulating all the beds. The characterization did not identify predictable-facies or predictable-fracture trends within the vertical stratigraphic column as originally hoped. Advanced logging techniques can identify productive beds in individual wells. A field-demonstration program was developed to use cased-hole advanced logging techniques in two wells and recompletion the wells at two different scales based on the logging. The first well was going to be completed at the interval scale using a multiple stage completion technique (about 500 ft [150 m] per stage). The second well will be recompleted at the bed-scale using bridge plug and packer to isolate three or more beds for stimulation. These recompletion will show which logs are most effective in identifying productive beds and what scale of completion is most cost effective. The third demonstration will be the logging and completion of a new well using the logs and completion scale or technique, most effective in the previous demonstrations.

Horizontal and vertical porosity trends based on density logs, and productive beds based on temperature and spinner logs, were mapped. There is no correlation between production, porosity, and facies distribution, in the Bluebell field. The combination of abundant source rock and sufficient depth of burial for maximum hydrocarbon generation is believed to control the location of hydrocarbons. Hydrocarbon generation controls the distribution of open fractures. The lateral extent of the open fractures is limited by the over pressuring caused by hydrocarbon generation and the rapid lateral facies change from sandstone into dense lacustrine mudstone and marlstone.

A novel stochastic approach was developed to generate fracture frequency distributions. In generating fracture frequency distributions, in addition to the "hard" fracture-frequency data, lithotype distributions were considered as soft data. The dependence of the fracture frequency distribution on rock type was reproduced accurately by using this approach. The fracture distributions thus generated were compared to networks generated through other, more conventional, geostatistical approaches. The fracture distributions generated using different approaches were incorporated into reservoir models and the flow performances were compared. Oil production from different models differed significantly, thus establishing the importance of generating "correct" fracture networks.

Numerical simulation of fractured reservoirs is computationally intensive. Hence, a parallel, multi-processor simulation approach was adopted. A parallel, fractured reservoir simulator was developed using a novel scheme called alternating direction implicit technique. For large problems, the simulator performed significantly faster with multiple processors than with a single processor. The performance test was carried out on SGI Power Challenge, a multiprocessor machine.

The first demonstration was designed to be a high-pressure, high-diversion three-stage, acid stimulation. Because of a leak in the tubing the operator could not treat the reservoir at as high a pressure as planned. Also, the treatment was pumped from a single packer location instead of three. Dipole shear anisotropy and dual burst thermal decay time logs ran before and isotope tracer log ran after the treatment were effective tools for identifying fractures and fluid-flow communication within the reservoir. Only the first 500 ft (152.4 m) of the gross perforated interval received acid, the lower 1000 ft 304.8 m) remained untreated. The demonstration did show how difficult it is to treat large vertical intervals from a single packer seat.

EXECUTIVE SUMMARY

The objective of the project is to increase oil production and reserves by the use of improved reservoir characterization and completion techniques in the Uinta Basin, Utah. To accomplish this objective, a two-year geologic and engineering characterization of the Bluebell field was conducted. The study evaluated surface and subsurface data, currently used completion techniques, and common production problems. It was determined that advanced cased- and open-hole logs could be effective in determining productive beds and that staged-interval (about 500 ft [150 m] per stage) and bed-scale isolation completion techniques could result in improved well performance.

Dipole shear anisotropy (anisotropy) and dual burst thermal decay time (TDT) logs were run before and an isotope tracer log was run after the treatment. The TDT log indicates hydrocarbons present in most of the sandstone beds in the logged interval. The TDT also shows about an equal amount of depletion in all the beds, including beds that are not perforated, indicating more vertical communication in the reservoir than anticipated. The anisotropy log indicates open fractures in many of the beds terminating at the bed boundaries. The tracer log shows the acid went above or below the perforations in some beds, corresponding to fractures indicated on the anisotropy log.

The first demonstration was designed to be a high-pressure, high-diversion, three-stage acid treatment of the Michelle Ute 7-1 well (section 7, T. 1 S., R. 1 E., Uintah Special Meridian). However, the tubing leaked and would not hold the high pressure so the acid treatment was applied from one packer location over a 1,550-ft (472.8-m) interval. The treatment did not result in a significant improvement in the oil production from the well.

Horizontal and vertical porosity trends based on density logs, and productive beds based on temperature and spinner logs, were mapped. There is no correlation between production, porosity, and facies distribution, in the Bluebell field. The combination of abundant source rock and sufficient depth of burial for maximum hydrocarbon generation control the location of hydrocarbons. Hydrocarbon generation controls the distribution of open fractures. The lateral extent of the open fractures is limited by the over pressuring caused by hydrocarbon generation and the rapid lateral facies change from sandstone into dense lacustrine mudstone and marlstone.

Characterization of fracture networks is one of the most important aspects of studying flow through fractured media. The methods used for fracture network generation have not been used in the context of the simulation of dual-continua models. These methods are also not conditioned to observed property distributions. Geostatistical principles were used to generate fracture density distributions by using not only spatial distributions of fractures frequency but by also taking into account the dependence of fracture distribution on rock type. Analysis of cores available from the field revealed that the fracture frequencies varied with rock type. Conditional simulations using the Markov-Bayes approach used frequency values and fracture frequency rock type dependence. The fracture networks thus generated were compared to those generated using Indicator Kriging and Gaussian simulations.

As the complexity of the reservoir models increases, the computational time required for numerical flow simulations also increases. Recent advances in the computer industry have led to the development of parallel machines that utilize multiple processors to perform a computational task. A new parallel numerical algorithm was developed using a technique called the alternating

direction implicit (ADI) method. ADI is particularly suitable for parallel implementation. For large problem sets, the parallel program showed significant speed-up compared to the single-processor, serial program.

Technology transfer activities for the year include information exhibits at one regional and one national petroleum industry meeting, one published abstract, and poster display at the national meeting. Inquiries and general discussion at the poster session and exhibitor booth indicate a strong interest by oil industry personnel. Meetings have been held with operators from the Bluebell field who continue to express strong interest in the projects activities and they have provided suggestions for each the demonstrations. Articles were published in the Utah Geological Survey *Petroleum News* and *Survey Notes* while daily activity reports for the first demonstration were posted on the Bluebell project home page.

1. INTRODUCTION

1.1. Project Status

The two-year characterization study of the Bluebell field, Duchesne and Uintah Counties, Utah, consists of separate, yet related tasks. The characterization tasks are: (1) log analysis and petrophysical investigations, (2) outcrop studies, (3) cuttings and core analysis, (4) subsurface mapping, (5) acquisition and analyses of new logs and cores, (6) fracture analysis, (7) geologic characterization synthesis, (8) analysis of completion techniques, (9) reservoir analysis, (10) best completion technique identification, (11) best zones or areas identification, and (12) technology transfer. Although portions of the characterization study are ongoing, the study has identified advanced logging techniques that can be effective in selecting beds for stimulation in old and new wells. A three-part field demonstration was developed to us the advanced logging techniques to selectively identify productive beds and test the effectiveness of treating at different scales (interval (about 500 ft [150 m]) and bed scale). The first demonstration has been completed.

The Michelle Ute 7-1 well (section 7, T. 1 S., R. 1 E.) was recompleted but mechanical problems resulted in inconclusive results. Cased-hole logs ran before and after the acid treatment have provided data for the reservoir characterization which will be valuable in designing the recompletion of the Malnar Pike 1-17A1E well (Sec. 17, T. 1 S., R. 1 E.), the second demonstration. As of September 30, 1997 (end of project year covered by this report) a workover rig had moved onto the Malnar Pike location, tubing was pulled, and the hole was being prepared for logging.

1.2. Geology and Field Background

The Uinta Basin is a topographic and structural trough encompassing an area of over 9300 square miles (24,000 km^2) (Osmond, 1964). The basin is sharply asymmetrical with a steep north flank bounded by the east-west trending Uinta Mountains and a gently dipping south flank bounded by the northwest-plunging Uncompahgre and north-plunging San Rafael uplifts. In Paleocene to Eocene time the Uinta Basin had internal drainage forming ancestral Lake Uinta. Deposition in and around Lake Uinta consisted of open- to marginal-lacustrine facies that make up the Green River Formation. Alluvial and fluvial red bed deposits that are laterally equivalent and intertongue with the Green River lacustrine deposits make up the Colton (Wasatch) Formation. The depositional environments are described in detail by Fouch (1975, 1976, 1981), Ryder and others (1976), Pitman and others (1982), Stokes (1986), Castle (1991), Fouch and Pitman (1991, 1992), Fouch and others (1990) and Franczyk and others (1992).

The Bluebell field is the largest oil producing field in the Uinta Basin. Bluebell is one of three contiguous oil fields; Bluebell, Altamont, and Cedar Rim (Fig. 1.1). The basin is an asymmetrical syncline deepest in the north-central area near the basin boundary fault. Oil is produced from the Eocene-Paleocene Green River and Colton (Wasatch) Formations near the basin center. The Bluebell field is 251-square miles (650 km^2) in area and covers all or parts of Townships 1 North, 1 and 2 South and Ranges 1 and 2 East and 1 through 3 West, Uinta Base Line (Fig. 1.1). More than 139 million barrels of oil (MMBO [19.5 million MT]) and nearly 182

billion cubic feet (BCF [5.2 billion m^3]) of associated gas have been produced as of September 30, 1997 (Utah Division of Oil, Gas and Mining records). The spacing is two wells per section, but much of the field is still produced at one well per section. The Roosevelt unit within the Bluebell field operates under the unit agreement. Although some wells have produced over 3 MMBO (420,000 MT), most produce less than 0.5 MMBO (70,000 MT).

The majority of the production and the focus of the demonstration is the Flagstaff Member of the Green River Formation reservoir (lower Wasatch transition [operator terminology]). The Flagstaff reservoir consists dominantly of carbonate and sandstone beds that were deposited in marginal- to open-lacustrine environments and is productive throughout most of the field. The Flagstaff is overlain by the alluvial-fluvial sandstone, siltstone, and shale (red beds) deposits of the Colton Formation. The Colton is overlain by the lower Green River lacustrine facies.

The complex heterogeneous lithology of the Colton and Green River Formations make it very difficult to identify which beds are actually potential oil producers. As a result, the operators have taken a shot gun approach to completing and recompleting the wells; they perforate 40 to 60 beds over a vertical interval of 1500 ft (460 m) or more, and acidize the entire interval. This completion technique is believed by the operators to leave many potentially productive beds damaged and/or untreated, while allowing water-bearing and low-pressure (thief) zones to communicate with the wellbore (Allison, 1995). Oil productive beds can be identified using advanced open- and cased-hole logs, allowing operators to perforate and treat smaller intervals resulting in more effective treatments. The demonstration is designed to show the effectiveness of treating more selective beds at different scales. The first demonstration was designed to treat a well at the interval scale (about 500 ft [150 m] per interval) and the second will be at the bed scale. The effectiveness and economics of the two different scales will be evaluated. The advanced logging techniques will be used on a new well to selectively perforate and treat the well at a much smaller scale than has been done in most Bluebell wells.

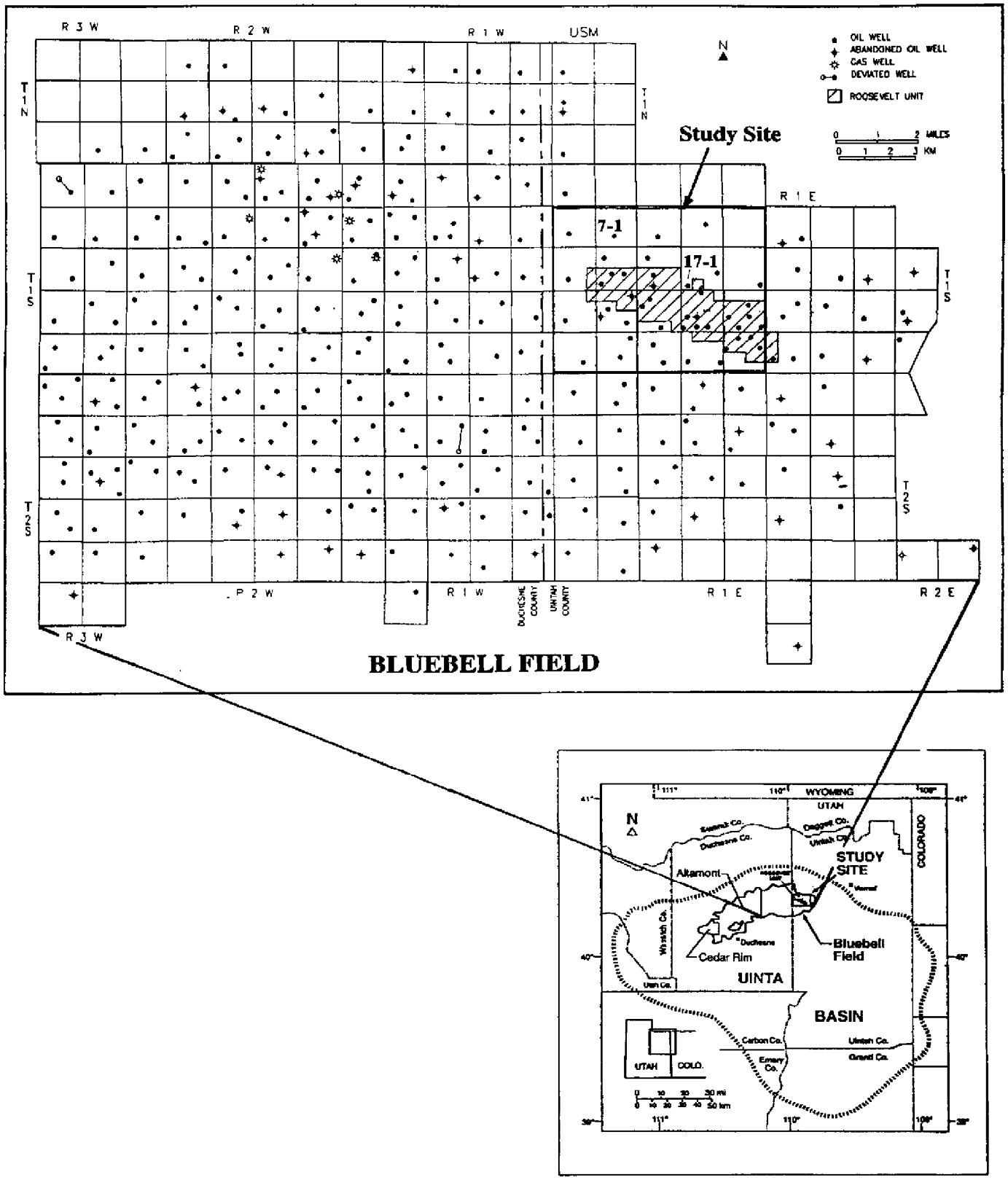

Figure 1.1 Location of Bluebell field, Duchesne and Uintah Counties, Utah.

2. HORIZONTAL AND VERTICAL DISTRIBUTION OF POROSITY AND OIL PRODUCTION

2.1. Introduction

Horizontal and vertical distribution of porosity and oil productive beds have no obvious correlation to each other, structure, or facies distribution in the Bluebell field. Porosity is best developed in the lower Green River Formation, generally 0 to 2000 ft (0-609.6 m) below the middle marker of Ryder and others, 1976. Porosity is poorly developed in the Flagstaff Member of the Green River throughout most of the field. Most oil production from the Flagstaff is above bed 23 (Morgan, 1997) locally known by operators as the 3-finger marker, but individual productive intervals do not correlate from well to well.

Fractures are an important part of the reservoirs in the Bluebell field as shown by Lucas and Drexler (1975) and Allison and Morgan (1996). Bredehoeft and others (1994) showed with fluid-flow modeling that the high reservoir pressure and open fractures of the deep reservoirs in the Altamont and Bluebell field could be caused by the generation of hydrocarbons. The apparent random nature of the fracturing in the reservoir both vertically and laterally, and the lack of any structural correlation, support the idea that fracturing in the deep Colton/Flagstaff reservoir is hydraulically, not structurally induced.

2.2. Horizontal and Vertical Distribution of Non-Fractured Porosity

Porosity data determined from density logs were used to plot vertical distribution of non-fractured porosity in selected wells (Fig. 2.1) in the Bluebell field. The plots of vertical distribution of porosity in each well were assembled into cross sections (Fig. 2.2) showing the horizontal and vertical distribution of porosity in a north to south and west to east (both structurally low to high) direction. Most of the porosity development is in the lower Green River Formation, 0 to 2000 ft (0-609.6 m) below the middle marker. Porosity is poorly developed in the Flagstaff Member of the Green River; the source of most of the oil production from the Bluebell field. Many of the wells that have produced over a million barrels of oil have very poor porosity development (Fig. 2.2, west to east line). Isochore mapping of individual beds (Morgan, 1997) does not correlate well with porosity distribution and is therefore a poor tool for predicting reservoir quality.

2.3. Horizontal and Vertical Distribution of Oil Production

Temperature and spinner logs were used to determine where the oil is coming from in wells in the 20-square-mile (50-km^2) study area. Most of the wells have about 40 to 50 beds perforated in a 1500-ft (460-m) vertical interval. Logs show that in most wells 90% or more of the production is coming from an average of five beds, generally in a 500-ft (150-m) or less vertical interval. Figs. 2.3 and 2.4 show the horizontal and vertical distribution of the productive beds in a north to south and west to east (both structurally low to high) direction. Most of the productive beds in the Flagstaff Member of the Green River Formation are above bed 23 (Morgan, 1997). The reason for this distribution is unknown but does not appear to be controlled

by a change in facies.

The distribution of productive beds does not show an obvious correlation structurally or stratigraphically between neighboring wells. The low ratio of productive beds to perforated beds is good evidence that wells are over perforated and most beds being treated are not contributing to the production. If the few beds that are productive can be correctly identified then both original completions and recompletions can be more effective and less costly, if only those few beds are treated. Operators argue that the production log is only a snapshot in time, and that the other beds might produce during different periods of a well's history. The few wells that have more than one production log do not show any significant shift over time in which beds produce but, there is not enough data to be conclusive.

2.4. Summary and Conclusions

Porosity is better developed in the lower Green River Formation compared to the Flagstaff Member. Porosity development appears to be localized and generally does not correlate to neighboring wells. Analysis of temperature and spinner logs shows that an average of five beds in a 500-ft (152.5 m) vertical interval are responsible for 90% or more of the oil production in most wells. Most of the productive beds are in the upper portion of the Flagstaff but the productive beds are rarely the same in two or more wells. The productive beds do not correlate to structural, sandstone isochore, or porosity trends.

Standard porosity, resistivity, and mudlog shows, cannot identify the primary productive beds in the Colton/Flagstaff reseervoir of the Bluebell field. As a result, over perforating and shot gun completions are common practice. Better definition of productive beds can be made using borehole imaging for fractures, and nuclear magnetics and thermal decay logs for fluid saturation. More restrictive perforating and acidizing based on the geophysical data should result in more effective and less costly treatments.

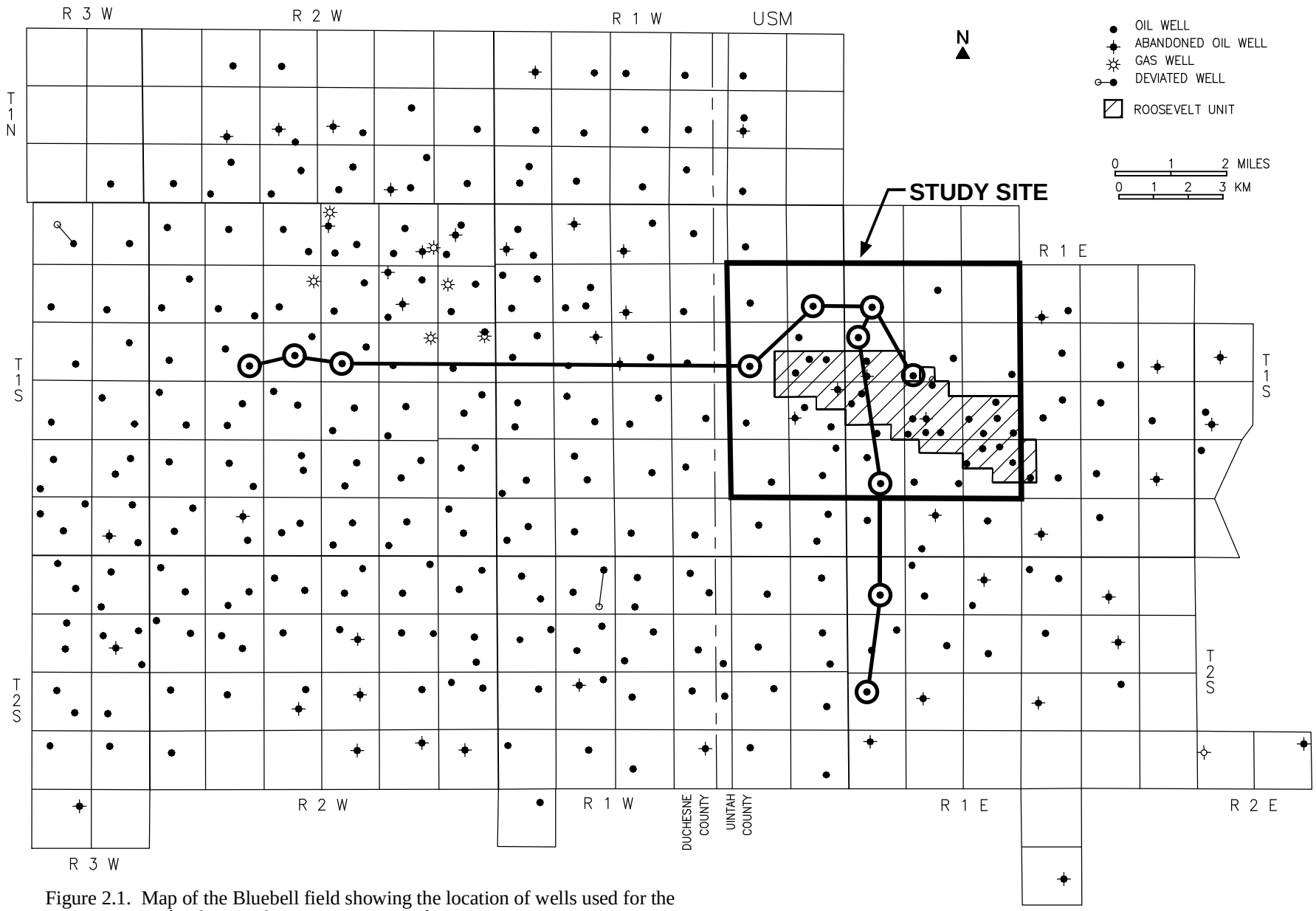

Figure 2.1. Map of the Bluebell field showing the location of wells used for the porosity-times-feet bar graphs cross sections in figure 2.2.

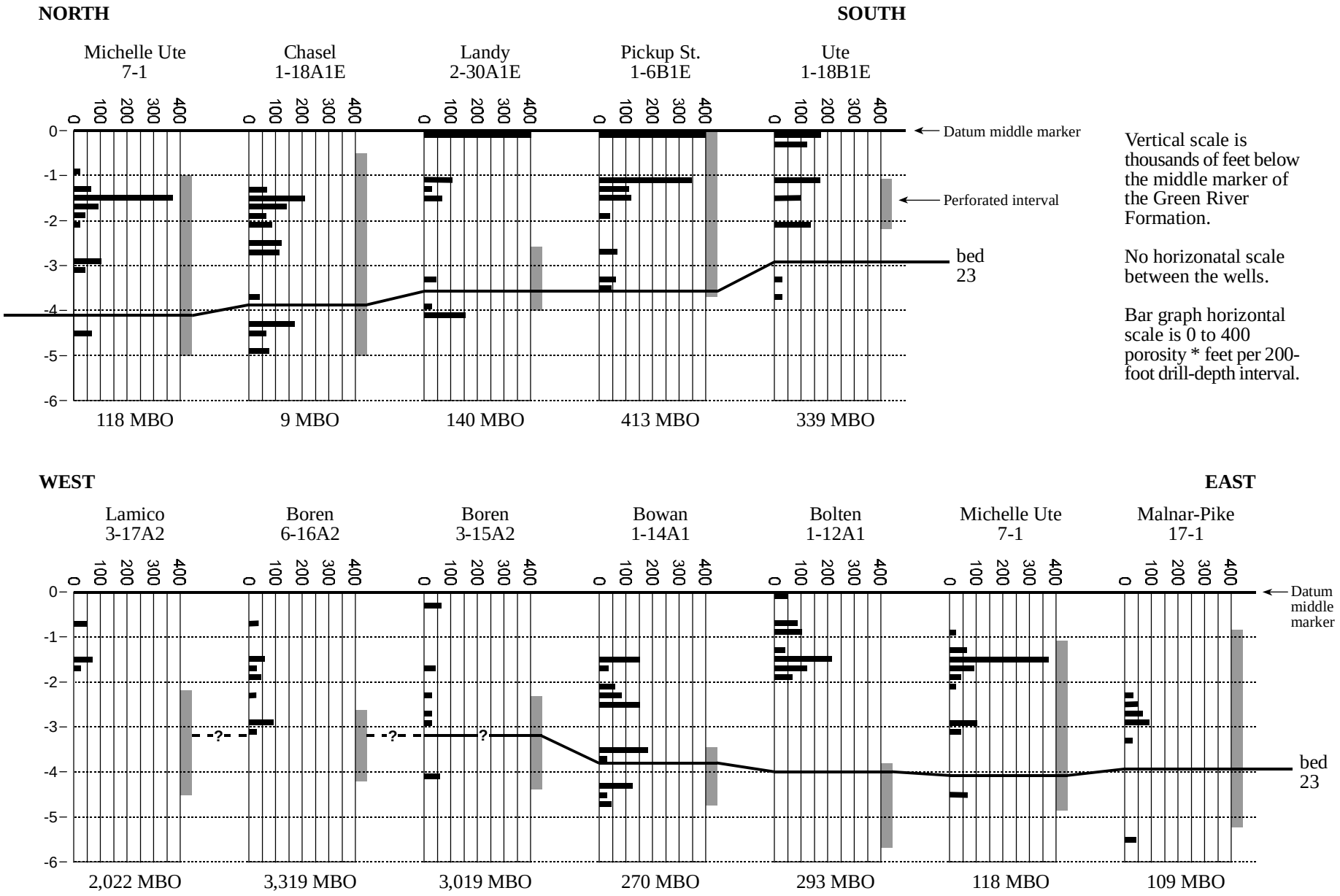

Figure 2.2 Well bar graphs showing porosity-times-feet per 200-foot drill-depth interval. See figure 2.1 for location of wells. Sea level datum.

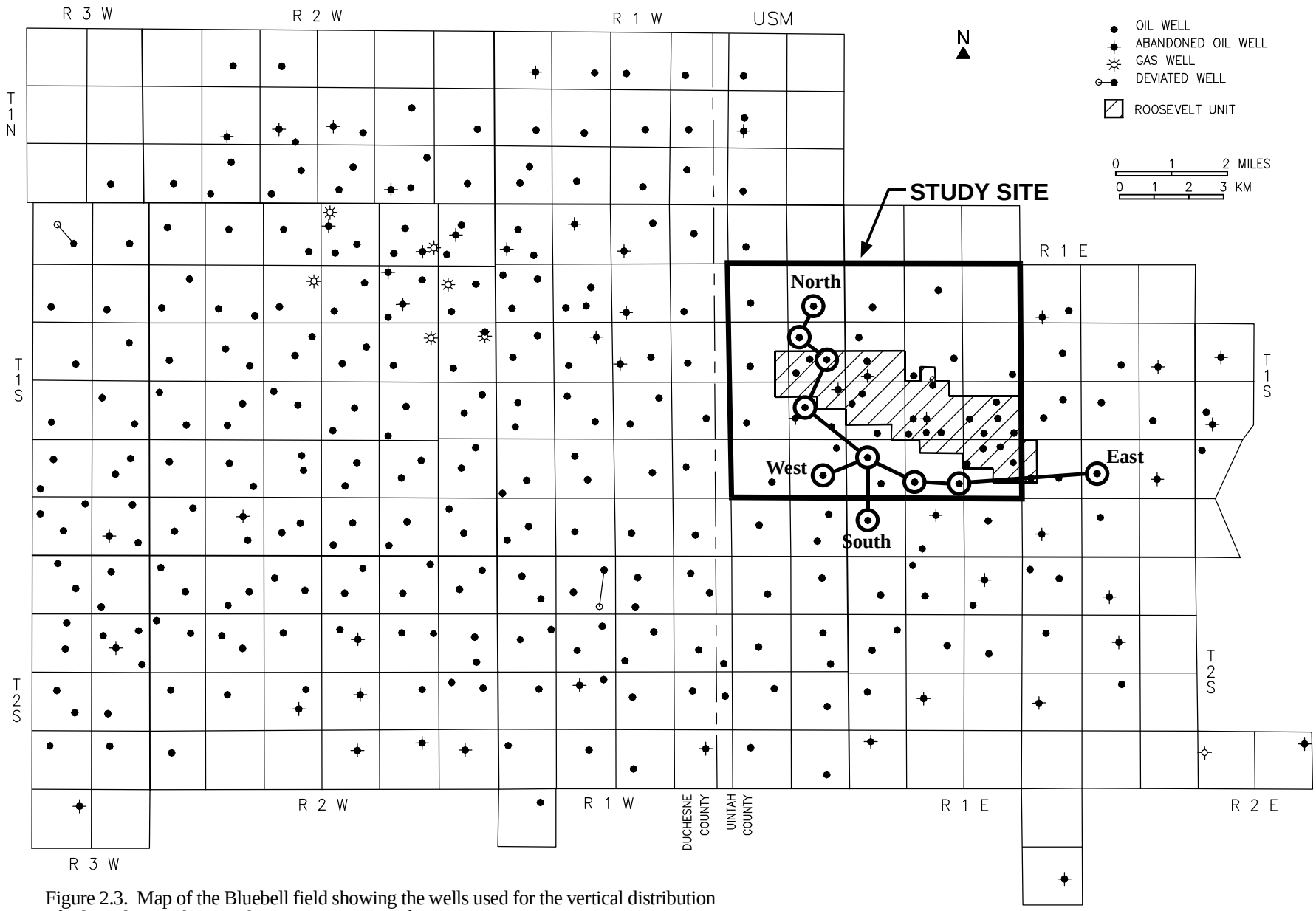

Figure 2.3. Map of the Bluebell field showing the wells used for the vertical distribution of oil production bar graphs cross sections in figure 2.4.

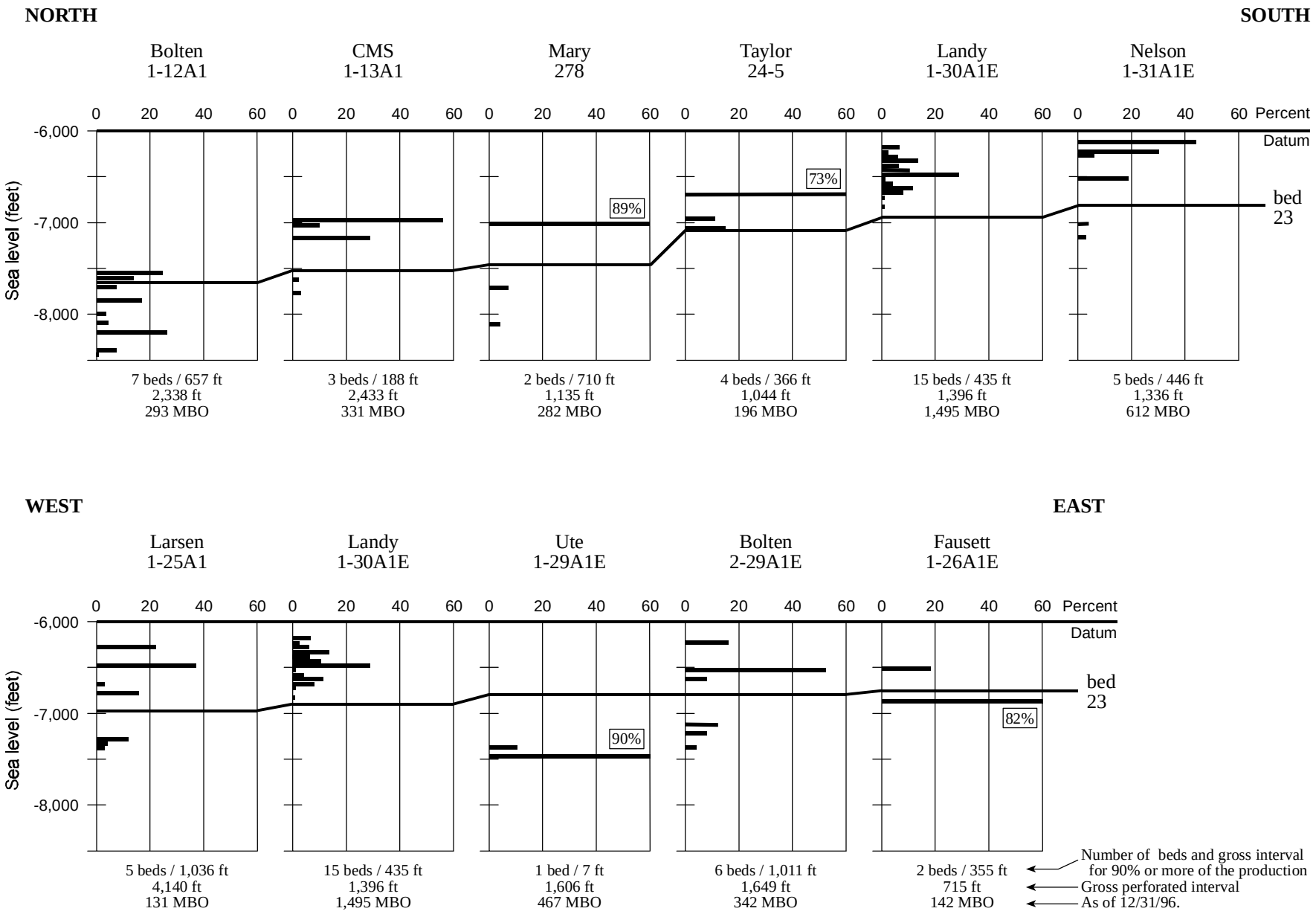

Figure 2.4 Well bar graphs showing the vertical distribution of the oil production from wells in the Bluebell field base on temperature and spinner logs. See figure 2.3 for location of wells. Sea level datum.

3. CHARACTERIZATION OF FRACTURE PROPERTIES

3.1. Introduction

Fractures largely control flow in a reservoir. It is therefore important to quantify fracture property distributions, reservoir wide. Fracture frequency is one of the most important fracture properties. Distributions of fracture frequency depends on the stress distributions and on rock types among other things. A novel approach based on geostatistical principles was used to generate fracture density distributions. Fracture density distributions were generated by using not only spatial distributions of fracture frequency but also by taking into account the dependence of frequency distributions on rock types. The fracture frequency data generated using this approach was compared to other stochastic approaches.

3.2. Background: Fracture Characterization Methods

Fracture frequencies over a spatial domain have been generated using several different techniques. Some of the most common methods are the:

1. Monte Carlo approach,
2. geostatistical approach,
3. fractal approach, and
4. process imitating approach.

The first three approaches were based on statistical principles. The generated networks were not conditioned to observed property values. Some of the fracture networks are generated using information about stress fields. Reservoir-wide stress distributions are difficult to measure. Most of these approaches have been used to generate fracture networks in two dimensions though some have extended the application to three dimensions. In all cases, extensive fracture characterization data was available. Another feature of these methods is that the area of study was small (300-30,000 ft^2 [100-10,000 m^2]).

In petroleum reservoir engineering, the scale of study is often larger than that used in generating networks using the first three approaches. Even after generation of fracture networks, integration of the fracture properties in reservoir models are another practical challenge. Often additional conditioning data are available which can be used to validate fracture properties distributions. Detailed analysis of the core data from the Bluebell field linked fracture frequency at different locations to rock types. This dependence of fracture frequency on rock types was used as soft conditioning data when generating frequency distributions over the entire study area. This was accomplished using the Markov-Bayes method (Deutsch and Journel, 1992).

3.3. Markov-Bayes Method

Simulation methods based on Gaussian models provide estimates of the unknown values. On the other hand, indicator based methods provide probability density functions of different categories at a location. These probabilistic estimates can be improved by taking into account secondary or soft data. The integration is performed through Bayes' rule of conditional

probability.

Bayes' rule states that if a random variable y is being conditioned using the value of another random variable x, the joint probability of (x, y) is proportional to the conditional probability of y given the occurrence of x, p(y|x). From this proportionality, we can write;

$$p(x,y)=p(y)p(x|y)=p(x)p(y|x) \qquad \text{(Eq. 3.1)}$$

Eq. 3.1 can also be written as,

$$p(y|x)=\frac{p(y)p(x|y)}{p(x)} \qquad \text{(Eq. 3.2)}$$

Eq.3.2 results in,

$$p(y|x)\propto p(x)p(x|y) \qquad \text{(Eq. 3.3)}$$

Eq. 3.3 is one form of the Bayes' Theorem of conditional probability.

The cumulative distribution function (cdf) of y is known *apriori*. In addition, 'n' observations of a second variable x, (x_1,…..,x_n) are also available. The probability distribution of x is dependent on the unknown values of y. The conditional cdf of x based on y is a function of x for fixed y. With the likelihood principle, the conditional cdf can be considered a function of y at fixed x. Bayes' Theorem says that the posterior cdf of y, p(y | x), which takes into account all the known data, is proportional to the prior cdf of y, p(y) multiplied by the likelihood function p(x | y). In other words:

$$\text{Posterior cdf} \propto \text{(Prior cdf x likelihood function.)} \qquad \text{(Eq. 3.4)}$$

The relationship above summarizes Bayes' rule.

Suppose sampling at a study site has resulted in m values of primary variable (u) and n values of secondary variable (v). The unknown values of u can be inferred from the posterior cdf of u. The posterior cdf is conditioned to available data.

$$\text{Prob}\{U(x) \leq u \mid u_1,\ldots, u_m, v_1, \ldots, v_n\} \qquad \text{(Eq. 3.5)}$$

The posterior cdf is obtained by applying Bayes' Theorem as follows.

$$\text{Prob}\{U(x) \leq u \mid m+n\} \propto f\{v \mid u\} \times \text{Prob}\{U(x) \leq u \mid u_1,\ldots,u_m\} \qquad \text{(Eq. 3.6)}$$

The data values on u and v are used to calculate the likelihood function f {v | u}. It is assumed that u and v are independent of each other. Then the above product can be converted to

a summation:

$$Prob\{U(x) \le u | (m+n)\} = \lambda_0 F(u) + \sum_{j=1}^{m} \lambda_j \bullet i(x_j, u) + \sum_{k=1}^{n} \gamma_k \bullet y(x_k, u) \qquad \text{(Eq. 3.7)}$$

In the above equation $I(x_j,u)$ are the indicators defined at the m locations where the primary variable is available.

$$I(x_j,u) = 1, \text{ if } U(x_j) \le u, = 0 \text{ if not} \qquad \text{(Eq. 3.8)}$$

The first term on the right hand side of Eq. 3.7, F(u), is the global expected value for a category. The first two terms on the right hand side of the Eq. 3.7 give the prior cdf of u based on the 'm' primary variables. In the absence of the secondary variable, the posterior cdf will be calculated based only on the primary variable and the procedure will reduce to that of simple indicator kriging.

The third term on the right hand side of Eq. 3.7 gives the prior probability of u conditioned to the secondary variable v.

$$y(x_k, u) = \text{Prob } \{U(x_k) \le u \mid v_1, \ldots, v_n\} \qquad \text{(Eq. 3.9)}$$

The sum of the indicators conditioned to secondary variable is the likelihood function. The m primary variables and n secondary variables are independent of each others. The unbiased nature of the estimates is assured by assuming that the sum of all the weights is 1.

In Markov-Bayes simulations, fracture frequencies, over the chosen model domain were generated by using the available fracture frequency data as the primary variable (hard data) and the rock type distribution as secondary data. The dependence of fracture frequency on rock type is thus included. The method is quite general and is limited only by the type of data available. The data that was available and used in generating these distributions has been discussed in detail in a later section.

3.4. Procedure for Markov-Bayes Simulations

If data are available on a primary variable u and secondary variable v, then the procedure for generating conditional cdf's using Markov-Bayes simulations is as follows.

1. The primary variable u is converted into indicators defined at K different cutoffs,$Ii(x_i, u_k)$, k = 1,….., K; I = 1, …., m.
2. The indicator variograms are calculated from all the available primary data for each cutoff.
3. The indicator variograms are used to calculate the covariances for each cutoff.
4. The secondary variable is discretized in L different classes, $v_1, \ldots, v_L$.
5. The u and v datasets are used to calculate the secondary indicators $y(x_j, u)$. A calibration scattergram of the primary values versus the secondary values is plotted. For

each class of the secondary variable, the scattergram values are used to calculate the probability distributions. An example scattergram is shown in Fig. 3.1.

6. The primary and secondary variable data values are also used to calculate the coefficients. These coefficients and the primary variable covariances are used to calculate the covariances and cross-covariances for the secondary variables approximated by the Markov hypothesis.

7. Once all the covariances are available, the posterior cdf's are calculated using the Bayesian updating formula defined in Eq. 3.7. A schematic of the procedure is shown in Fig. 3.2.

The procedure described above does not depend on the distribution of the primary or secondary variable. The secondary variable could be continuous or discrete. The primary variable can be continuous like porosity values and the secondary variable can be discrete like rock types.

3.5. The Data Set

The Markov-Bayes simulation technique was used to generate fracture density distributions for a study area in the Uinta Basin. Analyses were performed on cores from ten wells in the Bluebell field. The well locations are given in Fig. 3.3. The study area extends for 3 mi (4.8 km) in the east-west direction and for 1 mi (1.6 km) in the north-south direction. Formations from which the cores were collected and respective depths are shown in Fig. 3.4. No information was available about the rock facies. A total of 489 ft (149 m) of core were available from all the wells. These cores were analyzed in terms of rock-type classification, porosity, permeability values, and fracture properties. Fracture orientations, relative frequencies, and nature of the fractures (open, partially closed, closed, and so forth.) were noted.

Petrographic analysis of thin sections from the available cores has been described by Wegner (1996) and Wegner and Morris (1996). This analysis identified seven prominent rock types. They are:

1. shale,
2. mudstone,
3. siltstone,
4. sandstone,
5. limy mudstone,
6. packstone, and
7. wackestone.

Of the seven rock types, sandstone and mudstone were the most abundant.

The core samples were analyzed for fracture frequencies, which were classified qualitatively into the following categories: (1) one to two, (2) occasional, (3) few, (4) moderate, (5) frequent, and (6) very frequent.

Fracture analysis also indicated that the distributions of fracture frequencies varied with the rock types. Figure 3.5 shows the fracture frequency distributions for seven different rock types as reported by Wagner (1996). The cumulative frequency distributions within each rock type for the six fracture frequency classes are compared in the figure. As can be seen from the

figure, the frequency distributions vary with rock types. This information was used to generate distributions of fracture frequency using Markov-Bayes simulations. The primary variable was fracture frequency, while rock type was the secondary variable.

The rock-type distributions were first generated using principles of indicator kriging. The variation in fracture frequencies with rock type was used along with the hard frequency data when generating fracture frequency distributions. The fracture frequencies were conditioned to hard fracture frequency data and soft rock type data. The hard and soft conditioning was performed by using Markov-Bayes principles described earlier.

3.6. Three Different Approaches Used

For comparison purposes, two more approaches were used to generate frequency distributions. As mentioned previously, Markov-Bayes simulations reduce to simple indicator simulations in the absence of secondary data. The second approach used the data on hard indicators to generate frequency distributions by sequential indicator simulations. These distributions were conditioned to the observed frequency indicators. The third approach used was sequential Gaussian simulations.

3.7. Comparison of Fracture Frequencies Determined by Using the Three Approaches

The cumulative distribution functions (cdfs) of fracture frequencies for these three approaches are compared with sample data in table 3.1. As can be seen from table 3.1, the cdfs found using Markov-Bayes simulations come closest to reproducing sample data. Indicator simulations are next best. The cdf calculated using sequential Gaussian simulations does not reproduce the data well.

The effect of soft conditioning on the fracture frequency distributions was also examined. Analysis of sample data had showed that the fracture frequency distribution varied with rock type. As a result, the cdfs of frequency varied with rock type. Soft indicators were calculated for fracture frequency distributions generated using the three methods. These indicators are compared with the soft indicators for the sample data for sandstone and shale in Figs. 3.6 and 3.7. As can be seen from the figures, the cdfs for the sequential Gaussian and sequential indicator simulations results do not change with the rock type. The cdf of each category is the same as the global cdf. The results for Markov-Bayes simulations capture the trends of fracture frequency distributions for various rock types. The trends in the frequency distributions are well captured through soft conditioning.

3.8. Generation of Porosity and Permeability Distributions

The principles of Markov-Bayes simulations were also used to generate distributions of porosity and permeability. Porosities and permeabilities were measured on a few samples from

some of the cores. Rock-type information was also available on these samples. The data set, which was limited to 21 samples is tabulated in table 3.2.

All of the available data was used to generate stochastic distributions of porosity and permeability. Due to the limited size of the data set, the following procedure was used to generate these distributions.

1. The measures of spatial variability were not calculated for both the porosity and permeability. It was assumed that the spatial variability of these properties was controlled by their geologic control, the individual rock types. Since the semi-variogram for sandstone was most continuous over the study area, it was used for both porosity and permeability distributions.
2. Indicators were calculated for three cutoffs for each property. The cutoffs were defined at the quartiles of the individual data sets. The global expected values of each category were calculated. Similarly, soft indicators based on different rock types were also calculated.
3. The rock type distributions were used as soft conditioning data.
4. With the above information, the distributions of porosity and permeability were generated using the Markov-Bayes simulations. Unlike the fracture frequency distributions, these realizations were not conditioned to any observed data. The generated values varied between the observed maximum and minimum values.

The cdf for three quartiles are compared with the sample values in table 3.3. The fracture frequency, porosity, and permeability realizations were all conditioned to the same rock-type distribution data set. Thus, distributions of all the properties were assumed to be controlled through the rock-type distributions. These data sets were used to develop reservoir models for flow simulations.

3.9. Reservoir Flow Simulations

Two-dimensional reservoir flow models were used to study the effect of the fracture frequency distributions generated using the three different approaches. Three different reservoir models were developed. The three models differed only in the approach that was employed in generating fracture distributions. The model consisted of a block in the y-direction, 20 blocks in the x-direction, and 54 blocks in the z-direction. The x , y, and z dimensions of the grid blocks were uniform at 264 ft (80.5 m), 264 ft (80.5 m), and 20 ft (6.1 m), respectively. The porosity and permeability values varied according to stochastically generated data. Simulations were performed using the dual porosity, dual permeability models. The fracture porosity was assumed to be constant over the entire reservoir at 0.05. The fracture frequency varied according to the stochastically generated values. Fractures were assumed to be vertical and were present only in the x direction. The fracture permeability was constant at 1.0 millidarcies. The initial oil saturation was 0.7 and water saturation was 0.3. The initial reservoir pressure was constant at 4000 pounds per square inch (psi) (28,000 kPa). There were two wells; one of the wells was a producer and the other was an injector. The wells were located at the two ends (east-west) of the model. Water was injected at a rate of 20 stock-tank barrels per day (STB/D [2.8 MT/D]). Injection and production were begun from the simulation start. The simulations were run for

1000 days. The cumulative oil production for the three models are compared in Fig. 3.8. As can be seen from the figure, the flow performance of the three models differ. The production and injection results for models whose fracture frequency distributions were generated through Markov-Bayes and sequential indicator simulations are similar and both are higher than the third model where the frequency distribution was generated through sequential Gaussian simulations. These results indicate that different stochastic methods for generation of fracture frequency distribution will result in different production results.

3.10. Summary and Conclusions

Different methods used for generation of fracture networks and fracture property distributions have limited use in petroleum reservoir characterization. Most of the methods generate property distributions which are not in the form suitable for conventional methods of reservoir model development and flow simulations (for example, using dual-porosity, dual-permeability approach). A new method for fracture property distribution has been suggested in this study. This method uses principles of stochastic simulations. Analysis of sample data from Bluebell field had shown that the fracture-frequency distributions were functions of rock types. This information was used as an additional constraint while generating fracture frequency distributions using Markov-Bayes principles. Two types of conditioning were used during the stochastic simulation procedure. The observed values of fracture frequency were fully honored (hard conditioning), while the rock type information was used for soft conditioning. The fracture-frequency distributions generated through this approach were compared with the distributions generated using principles of sequential Gaussian simulations and sequential indicator simulations. It was shown that by soft conditioning, the dependence of fracture-frequency distribution on the rock type can be duplicated. The frequency distributions generated through the other two approaches did not reproduce this important trend. Reservoir models were developed with the fracture frequency distributions generated through these three approaches. The flow behaviors of these three reservoir models, as expected, were different as discussed in section 3.9.

The fracturing information available in most fields is limited. However, typically more information is available about rock types, and other petrophysical properties. If it is possible to link the fracturing tendency to other more abundantly available properties, then a systematic stochastic approach, such as the Markov-Bayes method can be used in generating field-wide fracture properties. Representation of fractures in the vicinity of wells has a major impact on completion techniques to be used in specific wells. For example, if fractures are abundant and communicating between various, completing in selected layers might be adequate in producing effectively from the field.

Table 3.1. Comparison of proportions of fracture frequency categories with sample data for three approaches.

	Sample Data	**Markov - Bayes Simulations**	**Seq. Gaussian Simulations**	**Seq. Indicator Simulations**
Category 1	0.1576	0.1636	0.2163	0.1465
Category 2	0.2153	0.2163	0.2682	0.2036
Category 3	0.5333	0.5688	0.5242	0.5153
Category 4	0.7567	0.7277	0.7008	0.7771
Category 5	0.8270	0.8056	0.7571	0.8398
Category 6	1.0000	1.0000	1.0000	1.0000

Table 3.2. Porosity and permeability data set.

Formation	**Rock Type**	**Porosity (%)**	**Permeability (mD)**
Flagstaff	Limy mudstone	2.82	0.461
Flagstaff	Wackestone	0.29	0.001
Flagstaff	Limy Mudstone	0.62	0.007
Flagstaff	Sandstone	1.27	0.024
Green River	Mudstone	0.27	0.002
Green River	Mudstone	0.30	0.004
Wasatch	Packstone	0.15	0.001
Wasatch	Wackestone	3.95	0.001
Wasatch	Sandstone	5.04	0.200
Wasatch	Wackestone	4.80	0.021
Wasatch	Sandstone	0.68	0.002
Wasatch	Mudstone	0.88	0.001
Wasatch	Sandstone	1.57	0.005
Wasatch	Mudstone	0.49	0.001
Green River	Shale	2.53	0.034
Green River	Sandstone	3.06	0.002
Green River	Sandstone	2.04	0.001
Wasatch	Wackestone	2.17	0.260
Wasatch	Wackestone	4.25	0.001
Wasatch	Packstone	3.20	0.000
Wasatch	Wackestone	1.67	0.001

Table 3.3. Comparison of cdfs for one output realization with sample data.

	Porosity Sample Data	**Porosity Realization**	**Permeability Sample Data**	**Permeability Realization**
Lower Quartile	0.0059	0.0068	0.3810	0.3057
Median Quartile	0.0157	0.0159	0.6191	0.6293
Upper Quartile	0.0310	0.0381	0.6667	0.6402

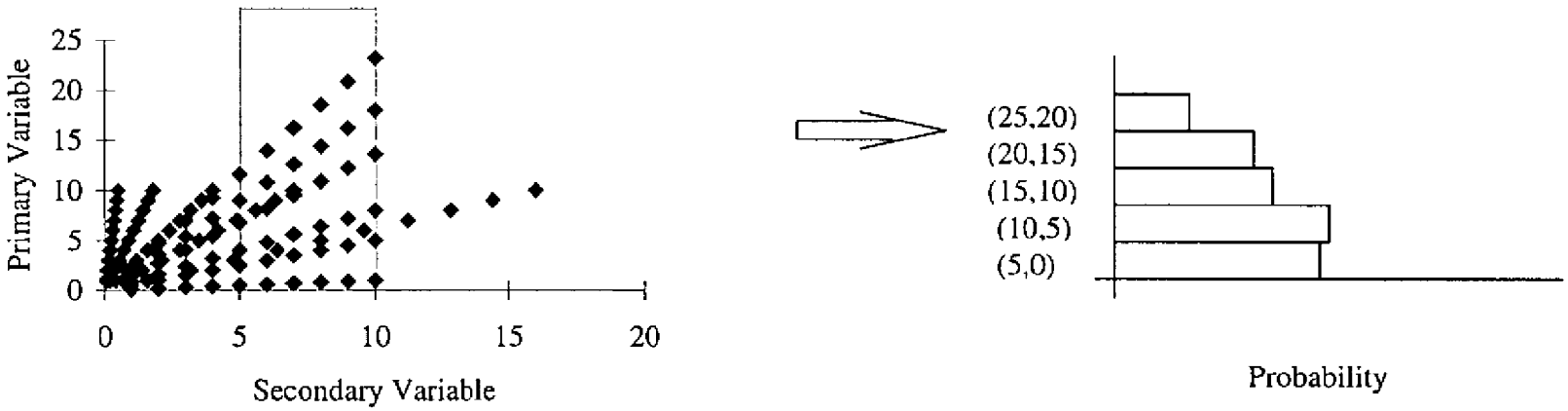

Sample Data

Prior Probability Distribution Function for Secondary Variable Class (5,10)

Figure 3.1. A scattergram and corresponding prior probability distribution function.

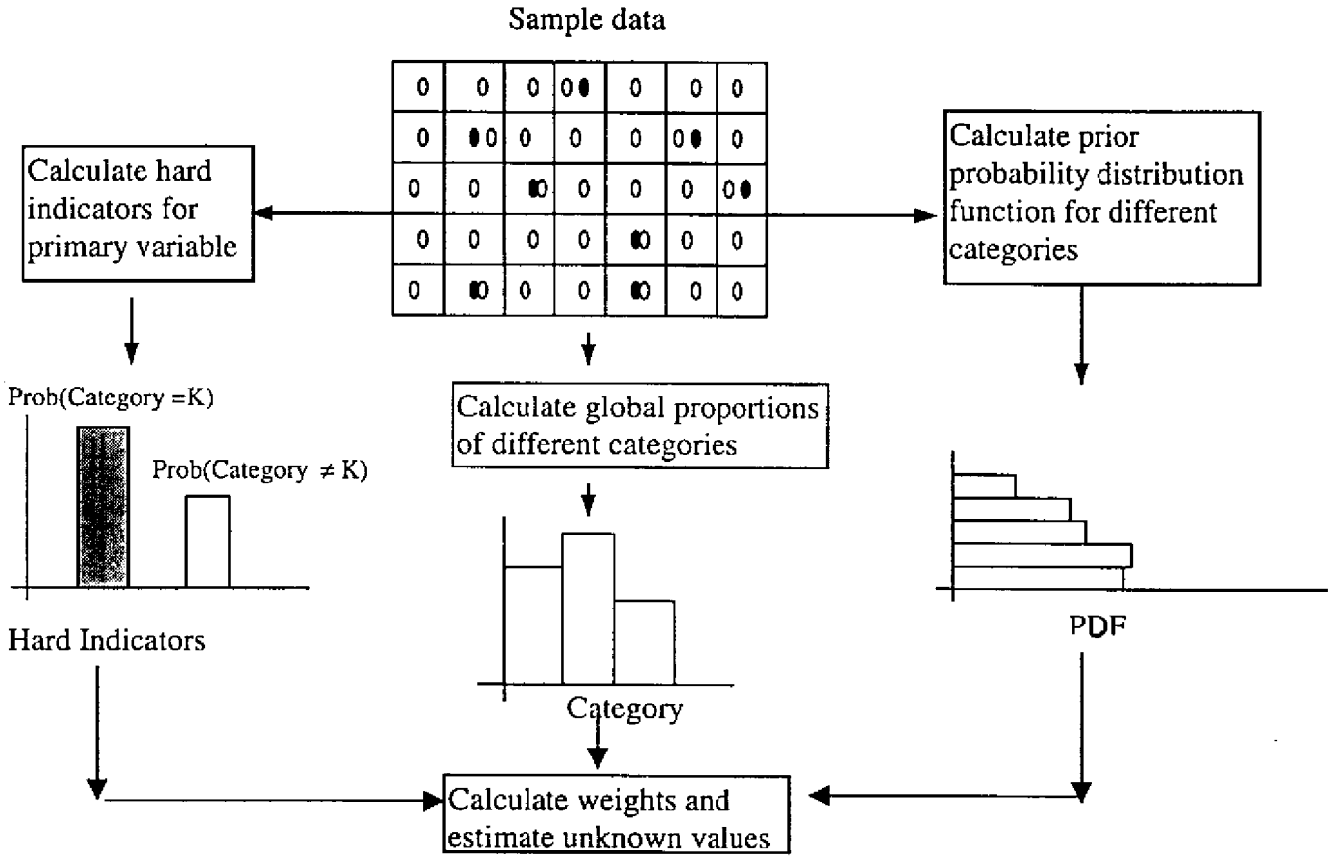

Figure 3.2. A schematic diagram showing the steps involved during Markov-Bayes simulation procedure.

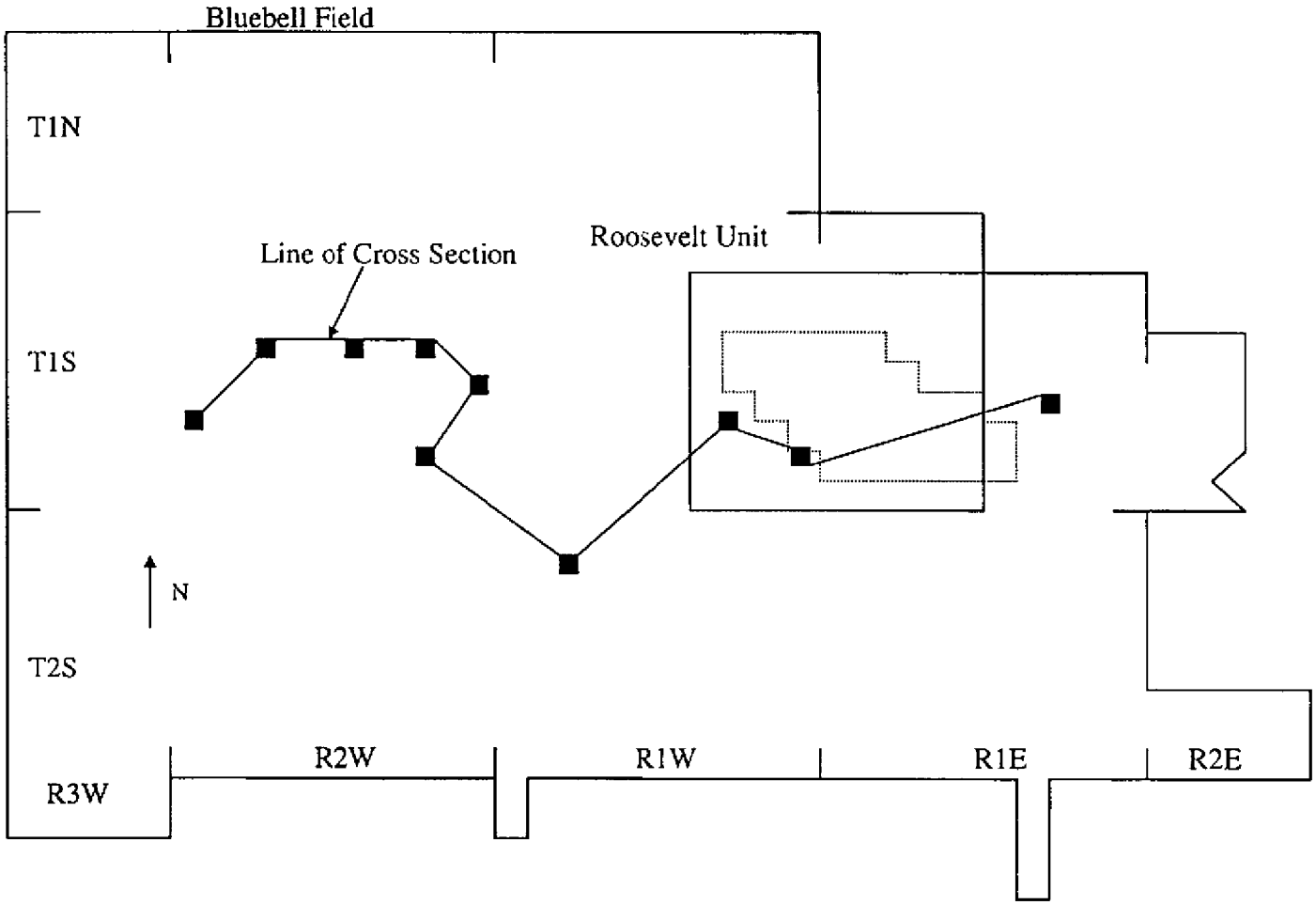

Figure 3.3. A map of the Bluebell Field showing the locations of core samples.

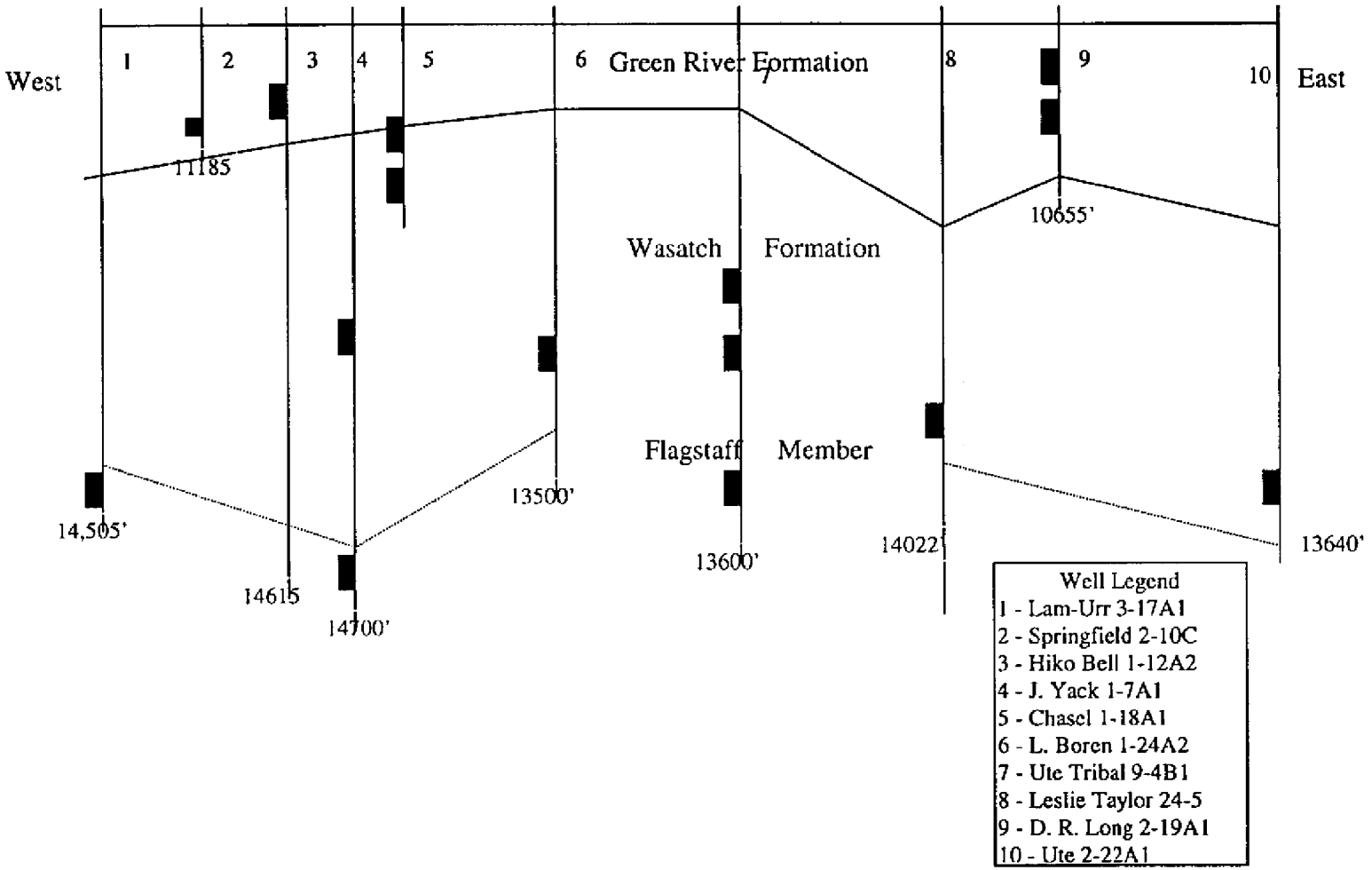

Figure 3.4. Cross section showing the formations and depths of core samples.

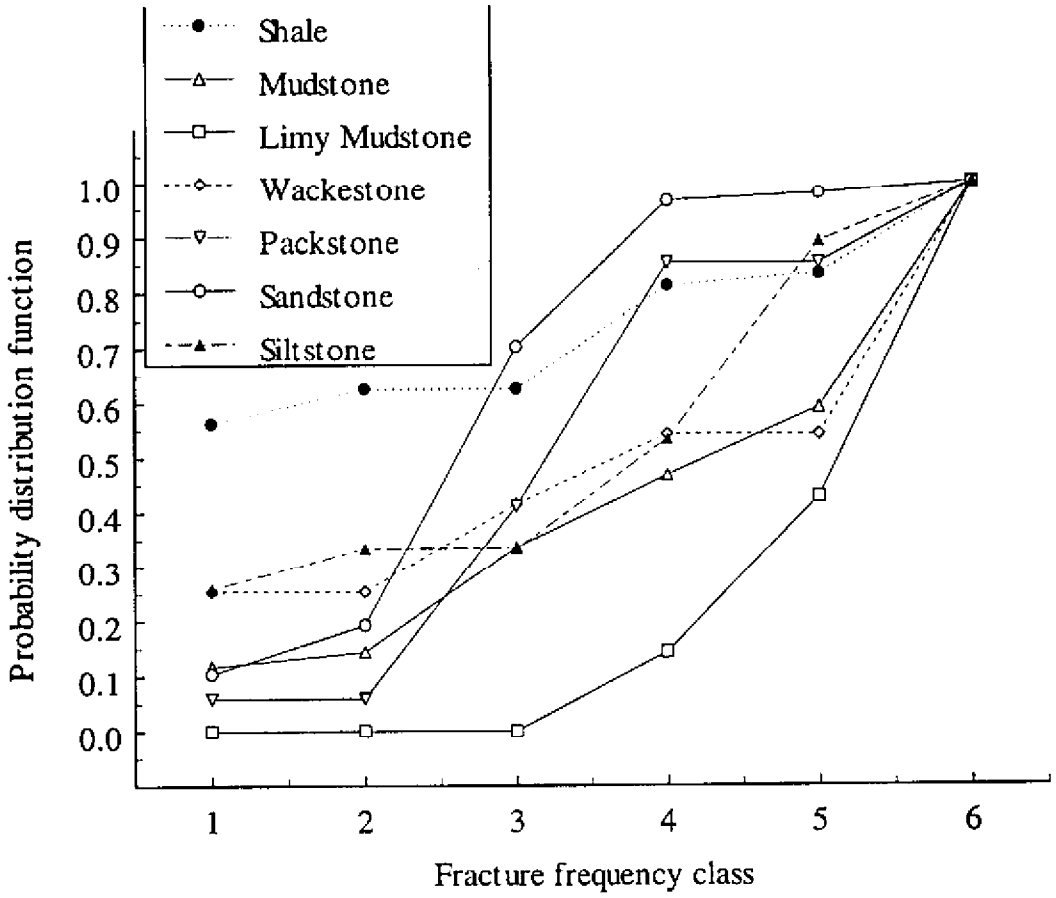

Figure 3.5. Fracture frequency distribution in different rock types.

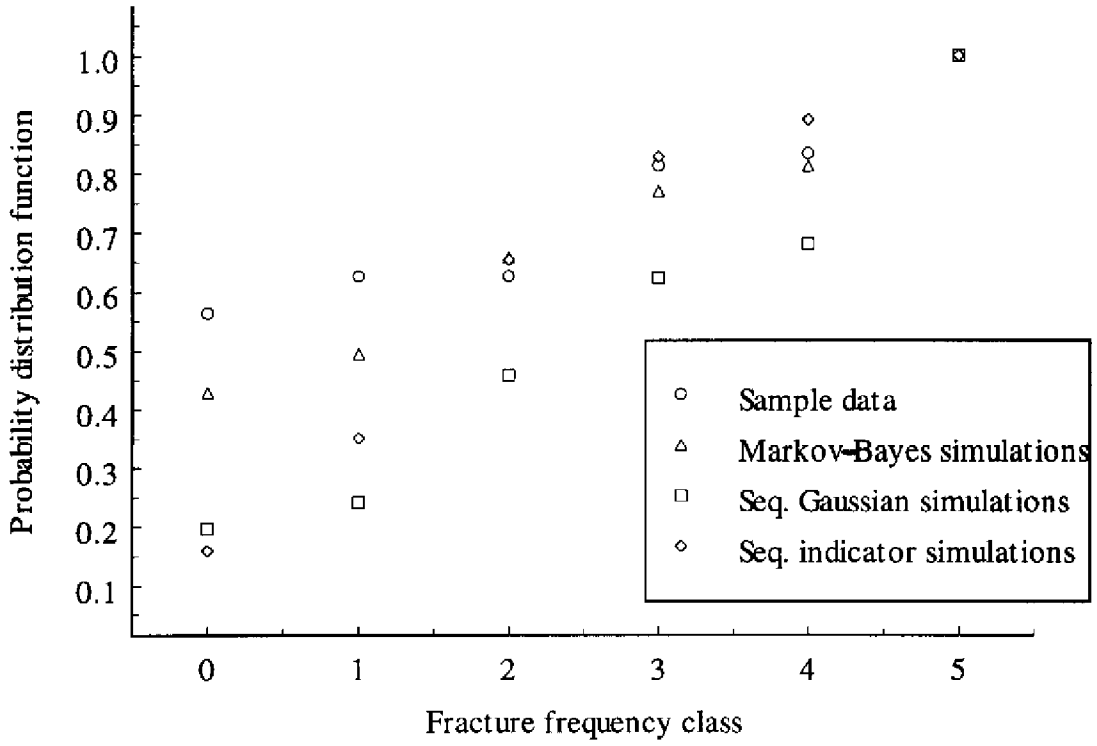

Figure 3.6. Comparisons of probability distribution functions for different fracture frequency categories for shale.

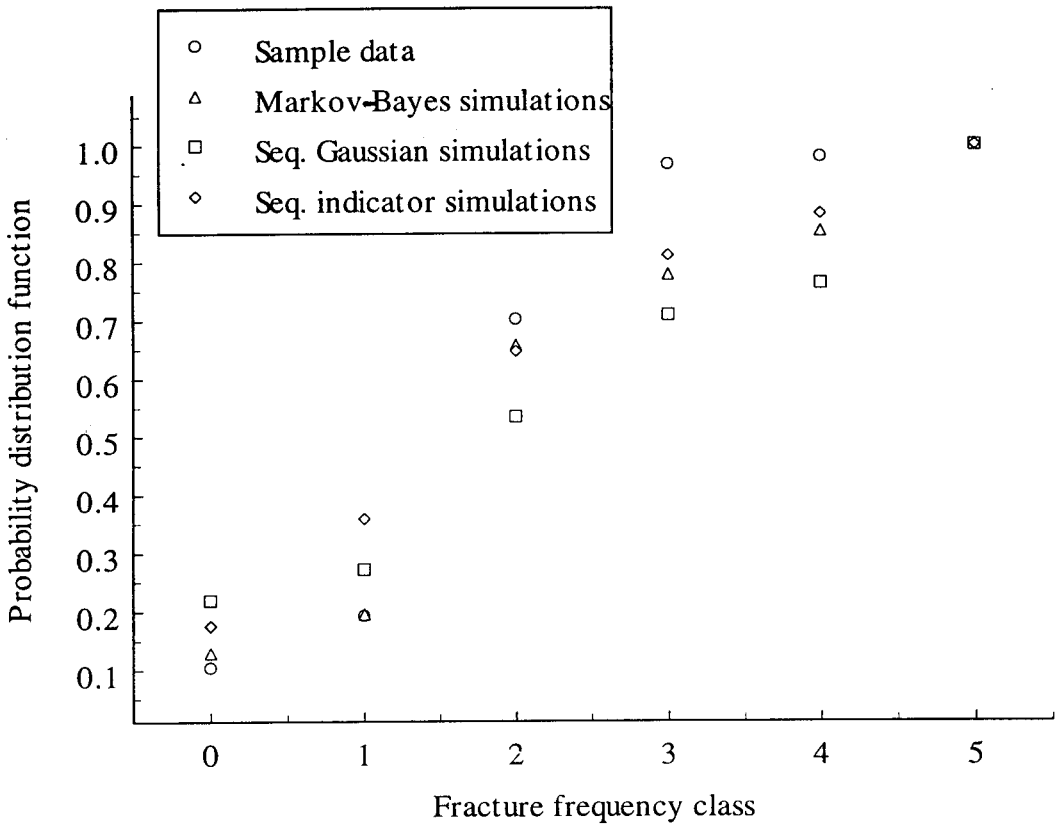

Figure 3.7. Comparisons of probability distribution functions for different fracture frequency categories for sandstone.

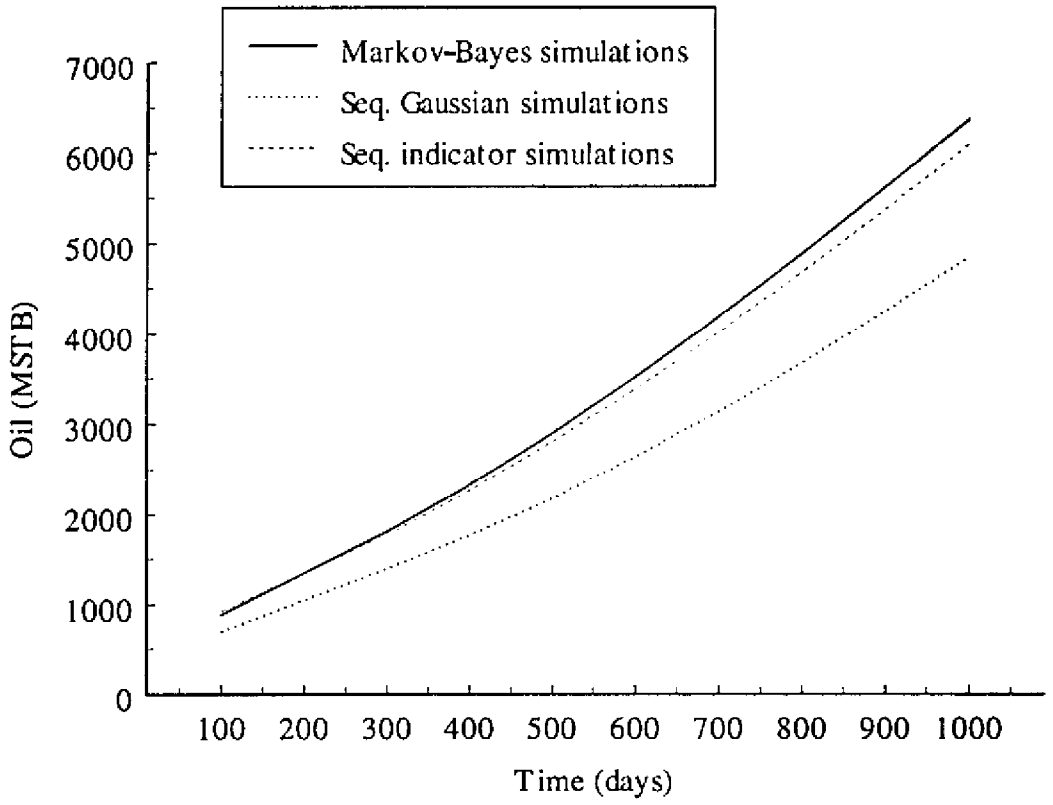

Figure 3.8. Oil production comparisons for the reservoir models developed with fracture frequency distributions generated through three different approaches.

4. DEVELOPMENT OF A PARALLEL FRACTURED RESERVOIR SIMULATOR

4.1. Introduction

The objective of developing a parallel processing reservoir simulator is to perform simulations on larger reservoir models accounting for reservoir heterogeneities at scales finer than those considered in current simulators. A larger reservoir model is necessary for the Bluebell field, where thousands of feet of producing intervals have to be considered in flow simulation. Flow simulations of heterogeneous fractured reservoirs as in the Bluebell field require a lot of computational time. One option of speeding-up the simulations is to divide the problem into a number of smaller segments and perform flow simulations on separate parallel processors. This requires a multiprocessor machine with the capability of allowing processor communications.

4.2. Parallel Computation and Reservoir Simulation

The parallel computation concept has been applied to reservoir simulation by a number of researchers. However, most of the implementations have been machine specific. One of the objectives of the development of parallel computer models in this project was to standardize the parallelization environment, so that the parallel code could be ported between machines. The eventual goal is to create a parallel simulator capable of running on a cluster of affordable workstations. This will make parallel computing more affordable and accessible to independent oil producers.

Parallel reservoir simulators have been implemented on both shared memory and distributed memory machines. At the University of Utah, Silicon Graphics Inc. (SGI) Power Challenge, a shared memory parallel machine and the IBM SP-2 of distributed memory architecture were used. These machines were used to streamline development of a parallel fractured reservoir code so that methods for porting the code to other workstation-cluster environments could later be developed.

The data partitioning in parallel computations can be achieved via strip partitioning (along data columns) or panel partitioning (along data rows) or box partitioning (three dimensions). Box partitioning is the most versatile of the methods. However, it requires more communications between processors than the other two approaches.

4.3. The Message Passing Interface – MPI Standard

Most of the parallel implementation in reservoir simulation has been machine specific. Message Passing Interface (MPI), a collection of small programs written to help the communication process in parallel computing, offers an attractive solution for standardization. MPI is a library of routines callable from FORTRAN 77 or C programs. The library specifies the names, calling sequences, and results of subroutines. The independent library format allows the source codes to be compiled on respective compilers and linked to the MPI library.

The fundamental function of MPI is to allow communication between processors. The six fundamental MPI functions are:

1. initialization,

2. identification of the total number of available processors,
3. assignment of processor rank,
4. sending data with appropriate attributes,
5. receiving data with the specified attributes, and
6. termination of the communication protocol.

Apart from these basic functions, MPI offers other functions for designing effective processor communication strategies and to optimize the parallel program.

4.4. The Fractured Reservoir Model

The fractured reservoir simulator was based on the dual-porosity, dual-permeability approach that is commonly used in modeling fractured systems. The discretized equations were solved using the well known implicit-pressure, explicit-saturation approach (IMPES). A serial version of the simulator was developed before development of the parallel version. The governing equations are coupled equations; the equation for fracture flow has matrix pressure terms and vice versa. These coupled equations were solved using a two-step procedure, conceptually depicted in Fig. 4.1. The fracture flow equation was solved for pressure in fractures first. In order to solve this equation the values for matrix pressures from the previous time step were used. With the new values for fracture pressures, the equation for flow through matrix was solved to get the pressures in matrix blocks at the new time step.

4.5. Development of the Parallel Version of the Fractured Model

The parallel version of the fractured reservoir code was developed using a domain decomposition or data partitioning method. Data dependency was considered before conversion to the parallel code.

Domain decomposition results in the distribution of the computational grid over available processors. The data dependencies need to be addressed before parallelizing the code. If the data that are dependent on their neighbors for certain computations are assigned to two different processors, communications will be required between the processors. Data dependency is very important in the solution of the tridiagonal equations which result when the line Gauss-Seidel method is applied to the discretized matrix and fracture equations. This method requires information from the neighboring nodes. In a two-dimensional computational grid, the regular Gauss-Seidel method calculates the unknown value as below.

$$f_{x,y}^{(k+1)} = b_{x,y} + f_{x-1,y}^{(k+1)} + f_{x+1,y}^{(k)} + f_{x,y-1}^{(k+1)} + f_{x,y+1}^{(k)} \qquad \text{(Eq. 4.1)}$$

As can be seen from Eq. 4.1, the new value at a grid point depends on the current values of it's south (x, y-1) and west (x-1, y) neighbors and past values from it's north (x, y+1) and east (x+1, y) neighbors. Suppose the two-dimensional data is distributed over a number of processors as shown in Fig. 4.2. The communications involved for processor M in the middle are shown in Fig.

4.3. In order to begin a local relaxation on this processor at time step 'n', it's south and west ghost boundaries must be updated from Processors W and S. Communications 1 and 2 send the east boundary points of Processor W and north boundary points of Processor S at time step 'n'. With these data points, Processor M updates all the data points at time step 'n'. Once all the data points are updated, Processor M sends it's east boundary points to Processor E and north boundary points to Processor N for their local relaxation at time step 'n' (communications 3 and 4). At the same time, it sends it's south boundary points to Processor S and west boundary points to Processor W for their local relaxation at time step 'n+1' (communications 5 and 6). Similarly when Processors N and E completely update their data points, they send their south and west boundaries respectively to Processor M for it's local relaxation at time step 'n+1' (communications 7 and 8). Thus the processor is involved in eight different communications in order to perform one update.

One of the disadvantages of the Gauss-Seidel method is that a processor can not start it's local relaxation unless it gets updated values from it's south and west neighbors. This results in idle processors at the beginning of the iterations. In the two-dimensional example above, at the beginning of the iteration, only Processor SW will perform local relaxation and all the others will be idle. Once it has completed calculations, then Processors W and S will start their local relaxations and so on. The Gauss-Seidel method is faster than the Jacob relaxation step, though the multicomputer implementation of it starts with idle processors. In order to overcome this problem a variation of Gauss-Seidel known as red-black Gauss-Seidel relaxation was developed. The grid points (x, y) are colored red if x + y is even and black if the sum is odd. When applying the Gauss-Seidel relaxation, grid points with the same color are relaxed simultaneously. The value of a grid point depends on the values of the grid points of different color in a five point stencil. Thus the pipe-lined nature of the Gauss-Seidel relaxation method is no longer a limiting factor in the red-black Gauss-Seidel method. One of the disadvantages of this method is increased number of communications. The number of communications is doubled since either only red or black boundary values are exchanged. Even though the number of communications is increased the size of the exchanged message is reduced.

The data dependency for the Line-Gauss-Seidel (LGS) method is a little different than the Point-Gauss-Seidel method. The LGS method results in the following system of equations.

$$a_x f_{x-1} + b_x f_x + c_x f_{x+1} = d_x \qquad \text{(Eq. 4.2)}$$

The advantage of a tridiagonal system of equations is that there are a number of pre-written solver subroutines available for such systems in advanced computational libraries like LAPACK. An example of the tridiagonal matrix which results from the above formulation is shown in Fig. 4.4. Suppose the data is partitioned such that half of the data nodes are assigned to one processor and the other half are assigned to a second processor. This data partitioning will result in two smaller systems of equations. As can be seen from Fig. 4.4, these smaller systems lose the tridiagonal nature of the larger system. Also these two systems are dependent on each other for computations. To solve for the value of f_3, the value of f_4 is necessary and vice versa. When these two systems are assigned to two different processors, the processors will not be able to solve the equations due to the data dependency.

An alternative approach was suggested by Hofhaus and Van de Velde (1995). An iterative method is used to solve the smaller system of equations. This iterative method is known as the modified half line Gauss-Seidel method. With this method the iterations can be performed on multiple processors concurrently. Instead of splitting the matrix as shown in Fig. 4.4, an alternative splitting method is used where the larger matrix is split into a set of tridiagonal matrices and another matrix which contains the coefficients for the coupling terms. This splitting is shown in Fig. 4.5. The advantage of this method is that the two smaller tridiagonal systems are completely independent of each other. Suppose the large matrix $\underline{A}$ is split in two smaller matrices $\underline{B}$ and $\underline{C}$, such that, $\underline{A}=\underline{B}+\underline{C}$. $\underline{B}$ contains the smaller independent tridiagonal matrices and $\underline{C}$ contains the coupling coefficients across data partitions. The original tridiagonal system of equations

$$Af=d \qquad \text{(Eq. 4.3)}$$

can be solved using an iterative method defined by above splitting as follows

$$Bf^{n+1}=d-Cf^{n} \qquad \text{(Eq. 4.4)}$$

The steps to implement the method are:

1. define the smaller system of equations resulting from data partitioning,
2. convert the smaller systems into tridiagonal systems,
3. start the solution of the tridiagonal system of equations independently on multiple processors,
4. use the solution from the past step for the coupling across the data partitioning, and
5. interactively solve the system of equations until the solution converges within some accepted tolerance.

For the example problem in Fig. 4.5, Processor 1 will solve the system of equations for f_1, f_2 and f_3, while Processor 2 will solve the system of equations for variables f_4, f_5, and f_6. Processor 1 will solve the equation for f_3 using the old value of f_4 and similarly Processor 2 will solve the equation for f_4 using old value of f_3. Once the system of equations are solved once, the new values of f_3 and f_4 will be communicated between the Processors. The error in the computed solution will be checked and if it is below a predefined tolerance then the Processors will go to next set of tridiagonal systems. If the error is above the tolerance the procedure is repeated.

With this iterative method the line Gauss Seidel relaxations algorithm can be implemented on multiple processors. Since all the processors start working on the system of equations simultaneously, there are no idle processors. During implementation the updated data values at the domain boundaries need to be communicated before the next iteration is performed by the processors. The parallel version of the serial code was based on this iterative tridiagonal solver to solve the tridiagonal system of equations generated by the implementation of the LGS method.

4.6. Development of Parallel Program

During the development of the parallel version of the programs, the communications requirements at different stages of the program were addressed. As mentioned before, the entire program was developed based on the domain decomposition method. The strip partitioning method was used for domain decomposition where the three-dimensional data set would be divided perpendicular to the x direction. The data was partitioned such that equal number of data points were assigned to each processor in order to have the same computational load on every processor. The development consisted of the following six steps which are shown sequentially in Fig. 4.6.

4.6.1. Initialization

The initialization step involves initialization of all the variables (MPI and non-MPI), definition of the configuration of the communicator, and definition of processor topology. The default communicator was used for the present program and the strip partitioning method was used for domain decomposition. The data was partitioned in the x direction. For a Processor with rank ‘n’, Processor with rank ‘n+1’ was defined as the ‘east’ neighbor and Processor with rank ‘n-1’ was defined as the ‘west’ neighbor. Once the initialization step was completed the input data file was read.

4.6.2. Read and Assign Input Parameters

The procedure used for reading the input data file and assigning the data to variables was different than for the serial code. In a parallel code, the data local to a processor is much smaller than the entire data set. It would be inefficient for each Processor to read the entire data set. This will not only require extra time but each Processor will also require a lot of storage for data which it will not be using. The data was read by one Processor, namely Processor ‘0’. Once the entire data file was read the data was communicated to all the Processors. There were two types of communications, which were dependent on the property types. The properties which would not depend on the grid locations, like fluid bulk properties were communicated by using the MPI_BCAST call. Only one call was required to broadcast values of such properties to all the Processors. The second type of properties were the location dependent properties like porosity and permeability for example. The values of these properties can vary from point to point. Since these properties are location dependent, only the Processor to which the data location is assigned needs to know the value of these properties. The values for these properties were communicated to each Processor separately. In order to facilitate the communication process some derived data types were defined. The derived data type was defined as a plane of data elements of same data types. Processor ‘0’ would then transfer the data values to each processor using these derived data types. Each processor would receive values of only those locations which were assigned to it. All the communications were performed using non-blocking send and receive operations. All of the parameters were thus transmitted to all the processors. Each processor then assigned property values to individual local property variables.

4.6.3. Formulate Fracture and Matrix Pressure Equations

This step was similar to the step in the serial code. Each Processor would calculate the various coefficient matrices in the fluid flow equations. These matrices were calculated only to the nodes that are local to the individual processor. These matrices were then used to formulate the system of fracture and matrix flow equations.

4.6.4. Solve Local Fracture and Matrix Flow Equations

The flow equations were solved using the modified half LGS method. This method resulted in tridiagonal system of equations on each processor. Each processor solved its local tridiagonal system of equations. For the domain boundary points, the values from previous time step or previous iteration were used. The solutions of the local tridiagonal systems were used to calculate the error in the local pressure estimates. The error was calculated as the difference between the left hand side and the right hand side of the flow equations. In order to calculate the error, communications between domain boundary points were required. All the local errors were combined to get the global error by using the MPI_ALLREDUCE operation. This operation is used to perform the global sum of some attributes from different processors. No other communication was required to calculate the sum of all the local errors. The value of the error was compared with the predefined tolerance limit. For this code, the tolerance was set at $1X10^{-7}$. If the global error was below this tolerance then the pressure values were updated to these new values, otherwise the procedure was repeated until the error reduced below tolerance. This iterative tridiagonal solution method was used to solve each set of grid nodes with constant y and z direction index. The procedure was looped over all the y and z values.

The new values of pressures were used to calculate the error in the pressure flow equation. Again each processor calculated the error local to it's computational domain and all the local errors were combined to calculate the global error. Communications were performed between neighboring processors to update the pressure values for domain boundary points before the local errors were calculated. The error value was checked with the tolerance limit for the pressure equations. These tolerances were also set at $1X10^{-7}$. The entire procedure was repeated until the global error was reduced below the tolerance.

The fracture pressure values were updated using this procedure. Once the new values of fracture pressures were obtained, the matrix pressures were calculated following same procedure. The updated pressure values were used to calculate the pressures at the boundaries of the entire computational domain.

4.6.5. Calculation of Saturation Values

The fracture and matrix pressures at the new time step were used to calculate the respective saturation values. The values of saturations at the domain boundary points were communicated between the neighboring processors. These saturations were used to perform the mass balance and the amount of fluids produced for the current time step. These steps constitute one time step for the simulation. The same procedure was repeated until the final time was reached.

4.6.6. Continue to the Next Step

Material balance checks are performed once the saturations are calculated. Fluids in place are calculated. The program is redirected to Step 1 for next time step calculations. If final time (user specified) is reached, the program is terminated.

4.7. Performance of the Parallel Program on a Shared Memory Machine

The parallel program was compiled and run on a SGI Power Challenge. The Power Challenge is a shared memory computer. It has 12 processors. The machine has two gigabytes of random access memory (RAM) and 12 gigabytes of hard disk space. The processors are MIPS R8000 chips with a clock speed of 75 megahertz.

The parallel program was run with two and four processors. Four different input models were used. The number of grid blocks for the four processor models were 16X16X16, 32X32X16, 64X64X16, and 128X128X16. The computation times required for various calculations mentioned above were used for comparison.

The times required to compute all the coefficients and set up coefficient matrices for formulation of the flow equations are compared in Fig. 4.7. For the two smaller models (16X16X16, 32X32X16 grid blocks) the time required to calculate the matrix coefficients are very small. These times do not change as the number of processors is increased. For the model with 64X64X16 grid blocks, the time required decreases gradually as the number of processors is increased. The change in the computational time is significant for the largest model (128X128X16 grid blocks). The time decreases significantly as the number of processors increase.

The times required to solve the fracture- and matrix-flow equations using the iterative tri-diagonal method are compared in Figs. 4.8 and 4.9. The time required to solve these equations increases as the number of processors is increased for the three smaller models. For the fourth model, the computational times decreases as the number of processors is increased. For the parallel program an iterative method is used to solve the tridiagonal system of equations. On the other hand the serial version does not use the iterative method to solve these systems. For the smaller models the time required increases due to the communications involved during the iterative process. For the serial code there are no communications involved while solving the tri-diagonal equations. For the largest model, solution of a tridiagonal system of equations for 128 blocks on a serial machine requires significant computational time. This time is reduced considerably as the problem size is decreased (64 for 2 processors, 32 for 4 processors). Even with additional time for communication during the iterative process, the total time required to compute the solution for the flow equations is reduced as the number of processors is increased.

The total time required to complete a single time step during flow simulations are compared in Fig. 4.10. For the two smaller models, the total time required does not change with additional processors. For the two larger models, the total time decreases as additional processors are used. The decrease is gradual for the model with 64X64X16 grid blocks, while it is significant for the model with 128X128X16 blocks. Computations of the coefficients require significant amount of CPU time. As the number of processors increase, the number of grid blocks assigned to each processors decrease which means fewer computations for calculations of matrix

coefficients.

4.8. Summary and Conclusions

A parallel fractured reservoir simulator was developed. A new technique known as the alternating direction implicit method, suitable for solving large linear systems on multiple processors was used in parallel implementation. A standardized, portable protocol called the Message Passing Interface was employed. For large problems, a considerable increase in computional speed was demonstrated on a shared-memory parallel machine. Fractured reservoir simulation can be performed by small to mid-size companies by using a cluster of workstations instead of large mainframe computers.

Models based on comprehensive representation of all of the identified correlatable layers in the vicinity of the project wells, Michelle Ute and Malnar Pike, were described in earlier annual reports. There were about 100 vertical layers in both of the models. Even when small areas in the vicinity of the wells were simulated, the computations took several minutes of central processing unit (CPU) time. Geologic characterization of the Bluebell field revealed numerous zones that were well correlated over long distances (miles). Field observations also indicated that oil was being drained over large areas and that the second well in a section did not perform as well as the first due to partial depletion. Hence, a large field model with fractures and with several layers will be necessary to estimate production potential of wells. The only possible way of simulating the model would be in parallel environment, with parts of the domain being assigned to different processors. To support predictive data, good production logs would be required, at a minimum. If characterization and modeling show the most promising zones, formation damage could be expected. It might be possible to over come the formation damage with recompletions.

The data from the recompletions will be carefully evaluated and modeled in the single-well mode. The effect of the treatments on each of the affected zones will be quantified in terms of pre- and post-treatment formation damage.

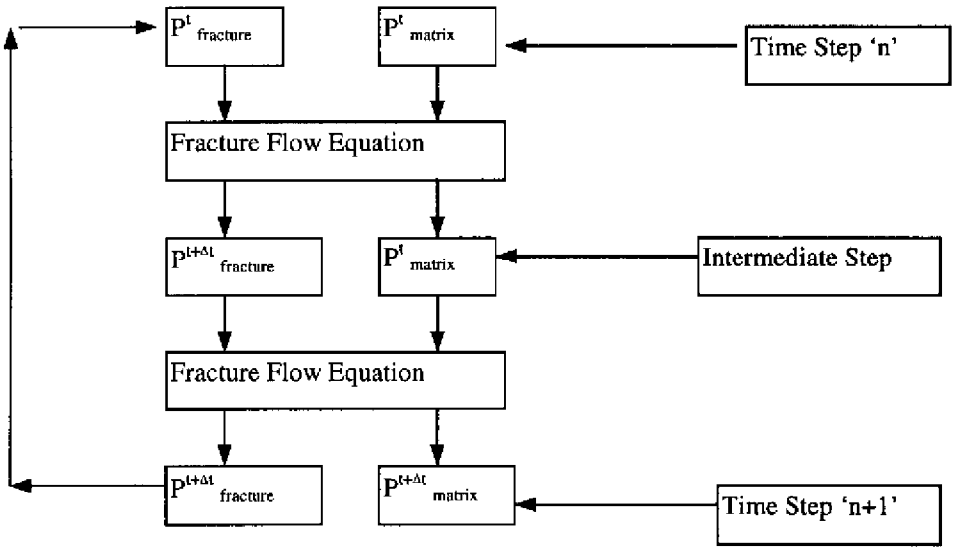

Figure 4.1. Conceptual diagram showing the approach taken to solve the pressure equations.

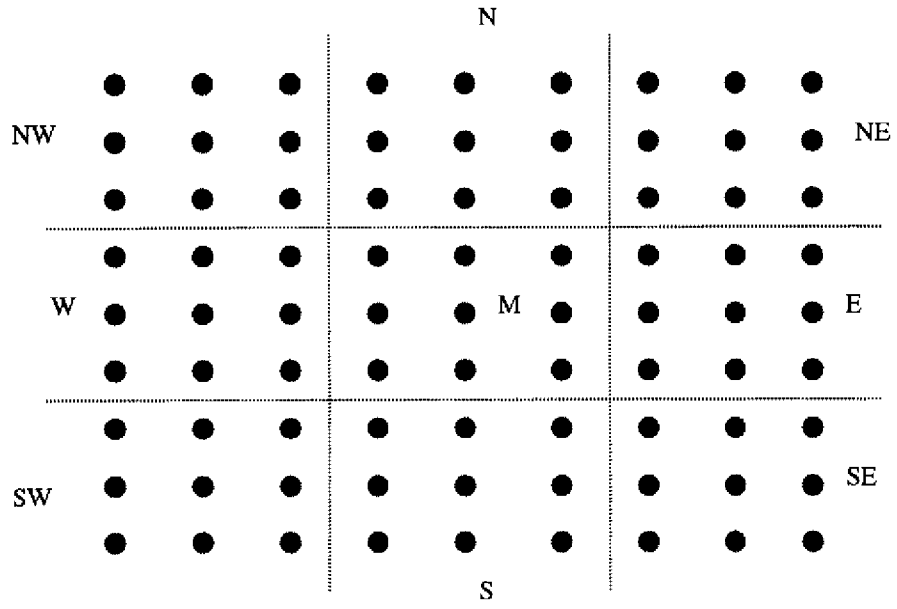

Figure 4.2. An example two dimensional computational grid distributed over a number of processors.

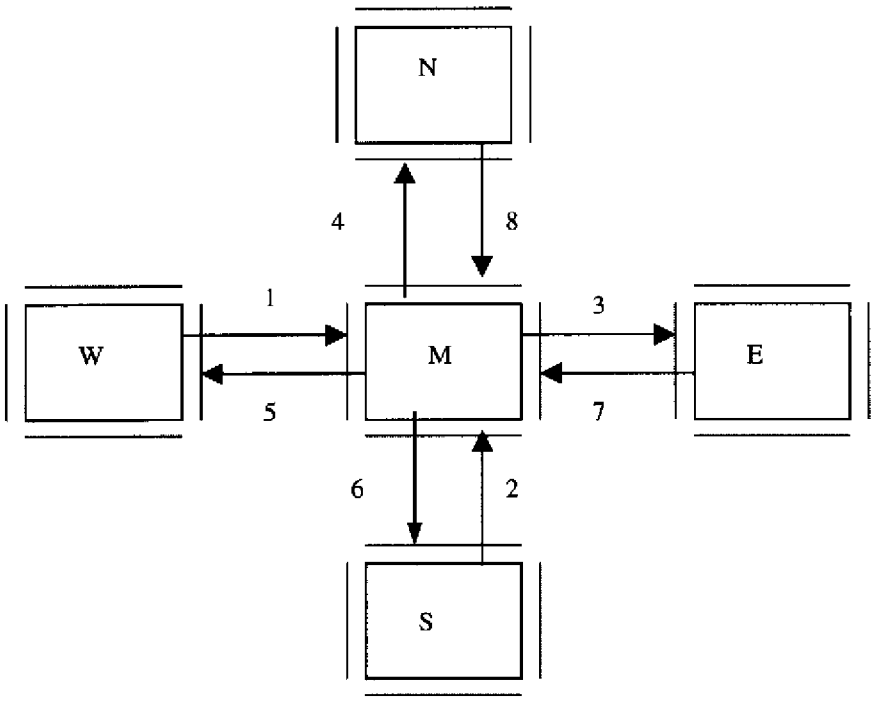

Figure 4.3. Communications involved during Gauss-Seidel relaxation.

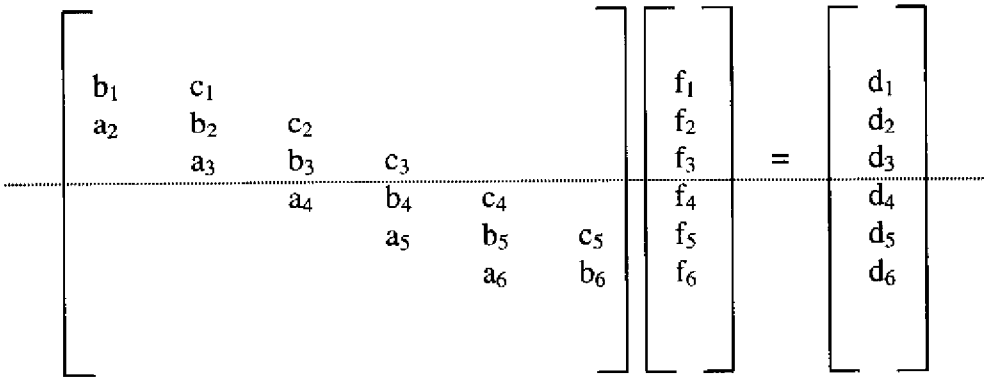

Figure 4.4 An example tridiagonal matrix splitting as a result of domain decomposition.

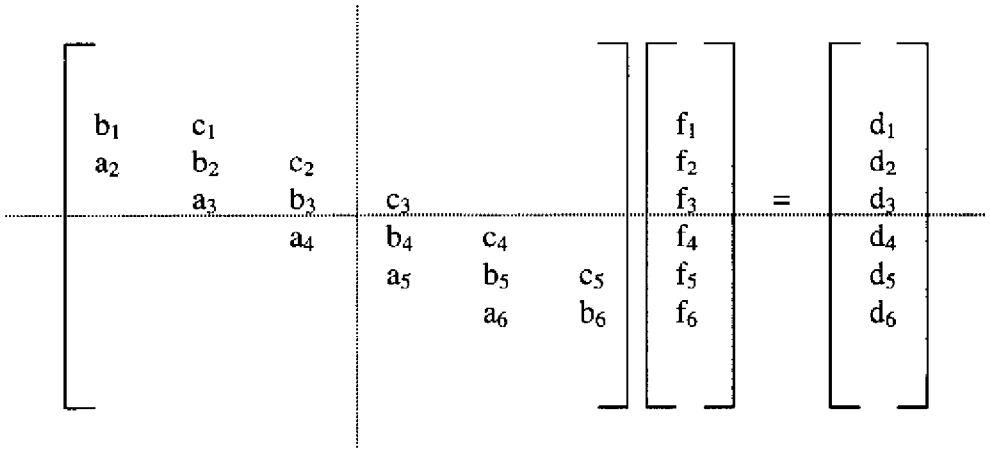

Figure 4.5. Matrix splitting for iterative tridiagonal solution method.

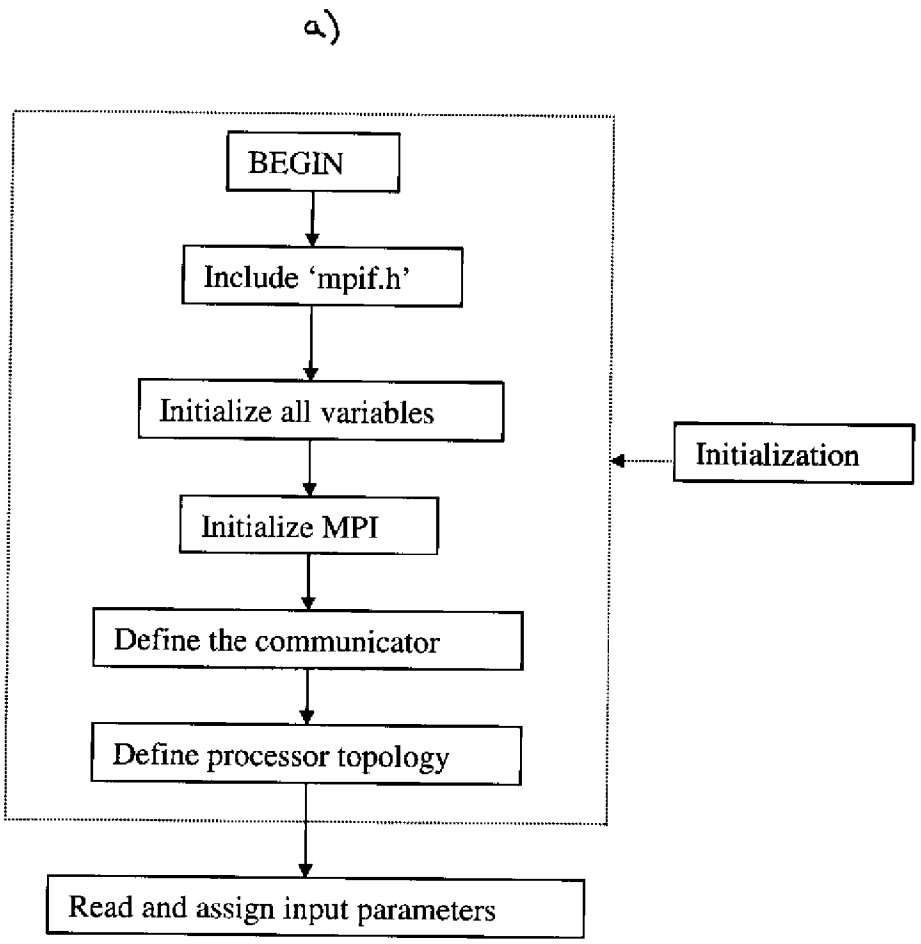

Figure 4.6. Basic steps involved in parallel flow simulations are shown here and on the next six pages: a) initialization, b) read and broadcast input data, c) formulate flow equations, d) solve for pressures, e) calculate saturations, and f) iterate to stop.

b)

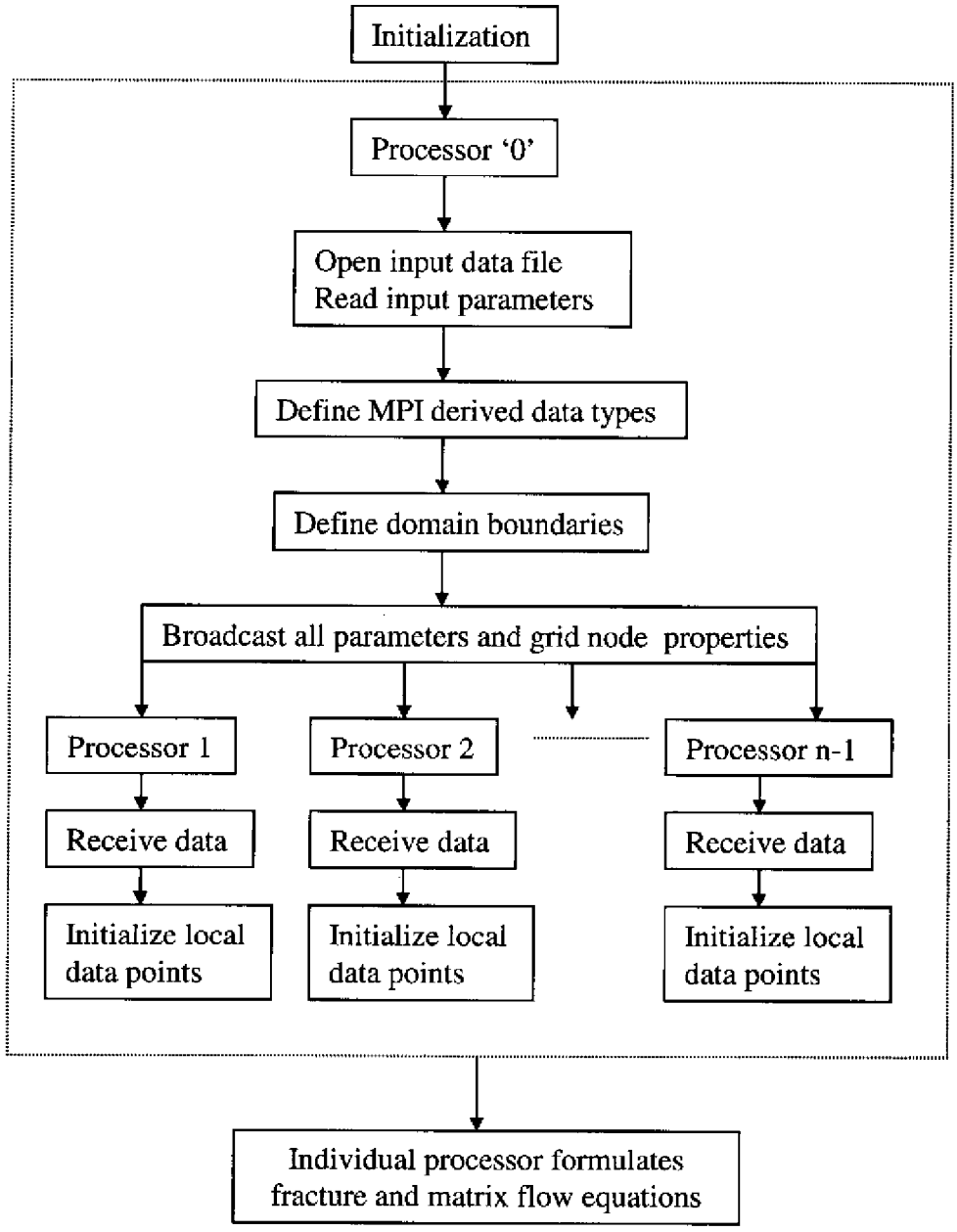
Initialization
Processor '0'
Open input data file
Read input parameters
Define MPI derived data types
Define domain boundaries
Broadcast all parameters and grid node properties
Processor 1
Processor 2
Processor n-1
Receive data
Receive data
Receive data
Initialize local data points
Initialize local data points
Initialize local data points
Individual processor formulates fracture and matrix flow equations

c)

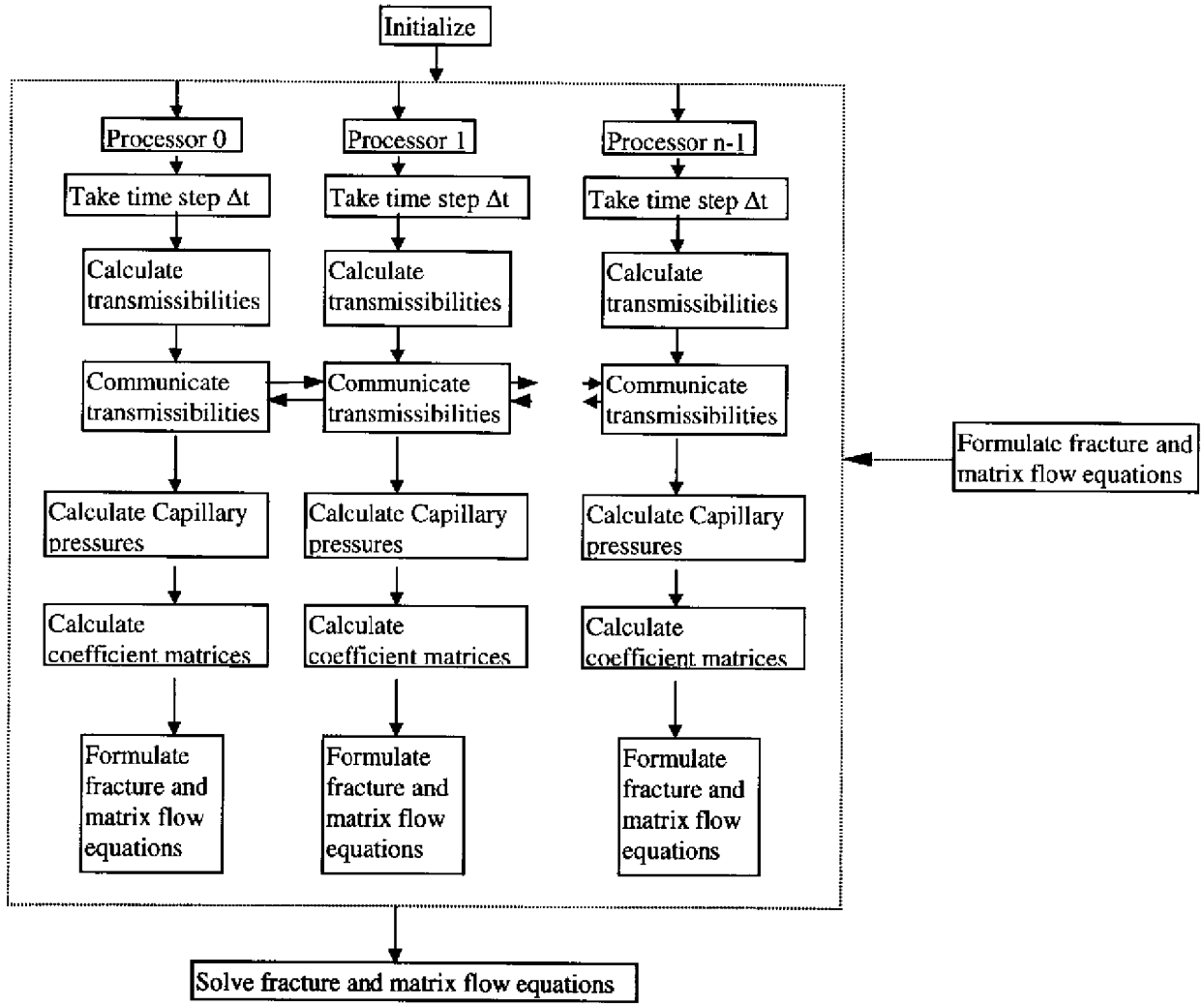
Initialize
Processor 0
Processor 1
Processor n-1
Take time step Δt
Take time step Δt
Take time step Δt
Calculate transmissibilities
Calculate transmissibilities
Calculate transmissibilities
Communicate transmissibilities
Communicate transmissibilities
Communicate transmissibilities
Calculate Capillary pressures
Calculate Capillary pressures
Calculate Capillary pressures
Calculate coefficient matrices
Calculate coefficient matrices
Calculate coefficient matrices
Formulate fracture and matrix flow equations
Formulate fracture and matrix flow equations
Formulate fracture and matrix flow equations
Formulate fracture and matrix flow equations
Solve fracture and matrix flow equations

d)

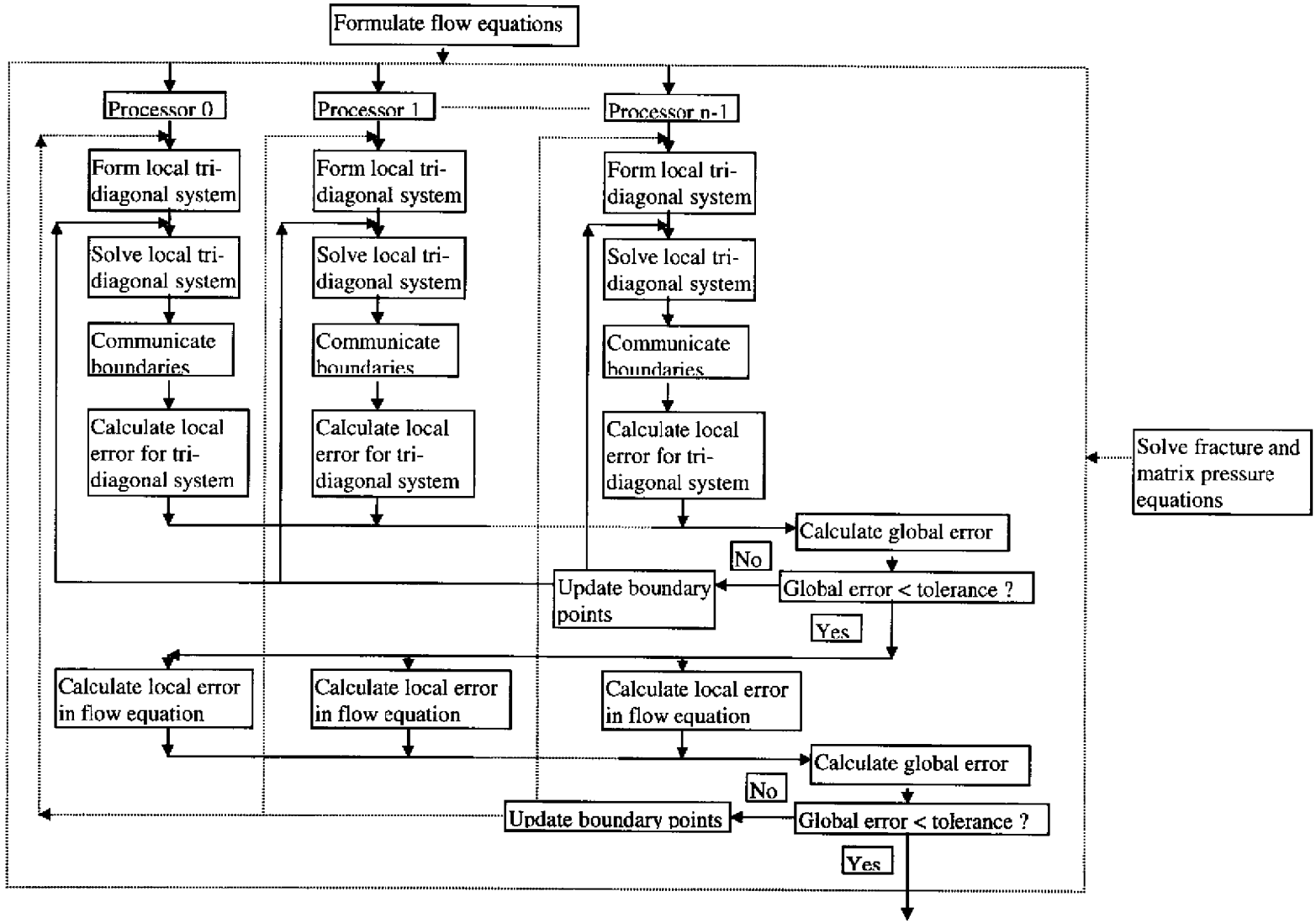
Formulate flow equations
Processor 0
Processor 1
Processor n-1
Form local tri-diagonal system
Solve local tri-diagonal system
Communicate boundaries
Calculate local error for tri-diagonal system
Calculate global error
No
Global error < tolerance ?
Update boundary points
Yes
Calculate local error in flow equation
Calculate global error
No
Global error < tolerance ?
Update boundary points
Yes
Solve fracture and matrix pressure equations

e)

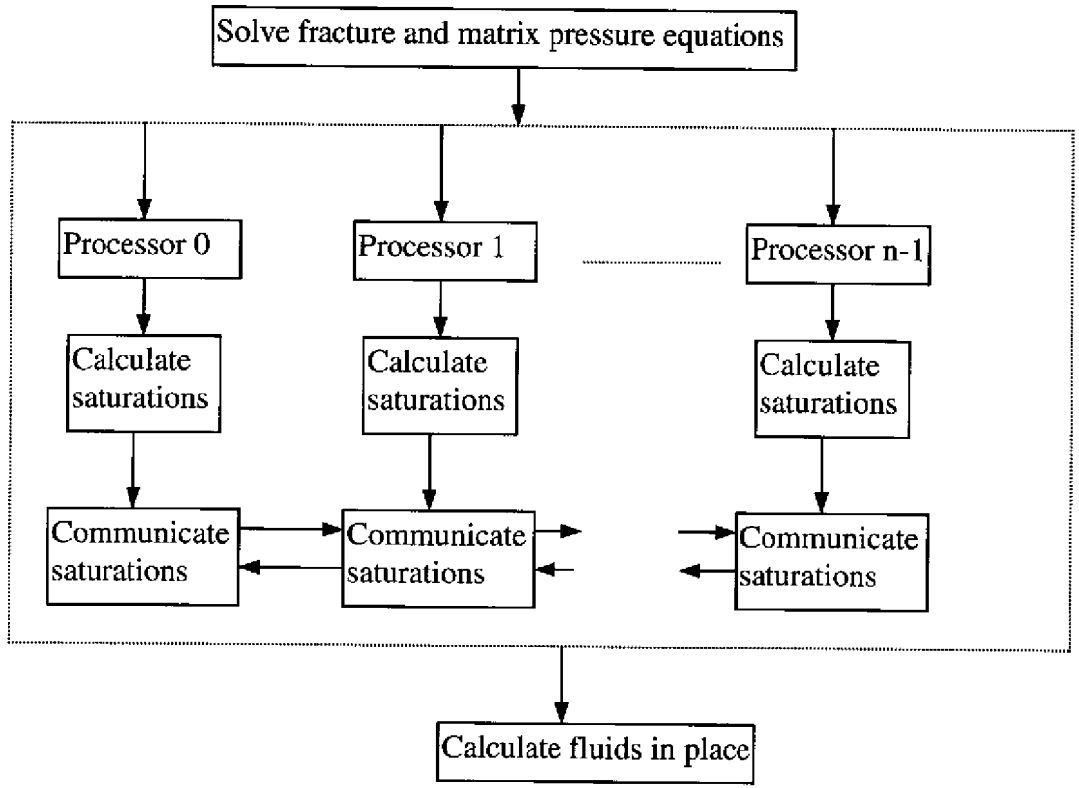
Solve fracture and matrix pressure equations
Processor 0
Processor 1
Processor n-1
Calculate saturations
Calculate saturations
Calculate saturations
Communicate saturations
Communicate saturations
Communicate saturations
Calculate fluids in place

f)

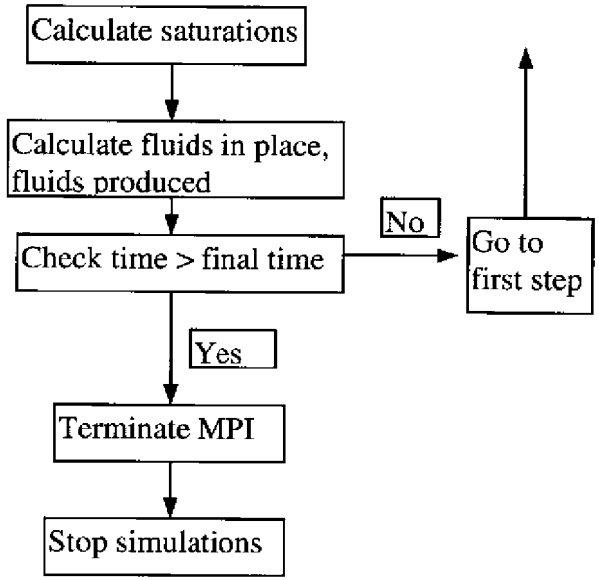
Calculate saturations
Calculate fluids in place, fluids produced
Check time > final time
No
Go to first step
Yes
Terminate MPI
Stop simulations

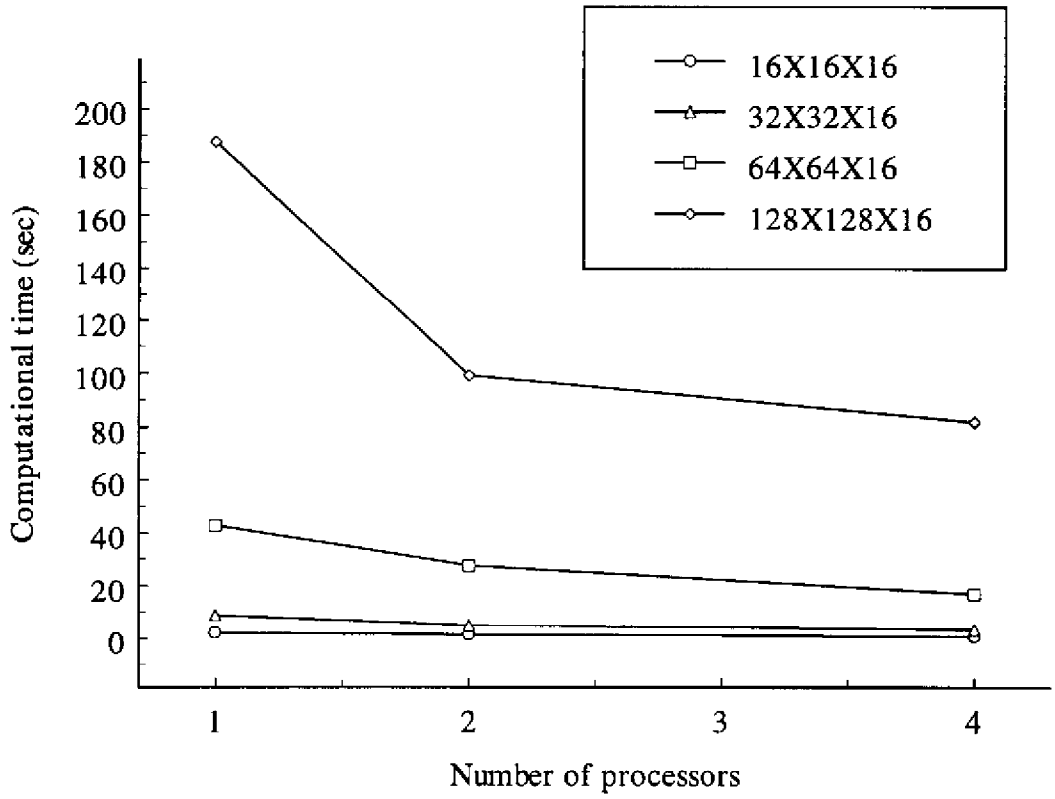

Figure 4.7. Comparison of computational time for the calculation of coefficient matrices for the serial program (1 processor) and parallel program (2 and 4 processors) on SGI Power Challenge.

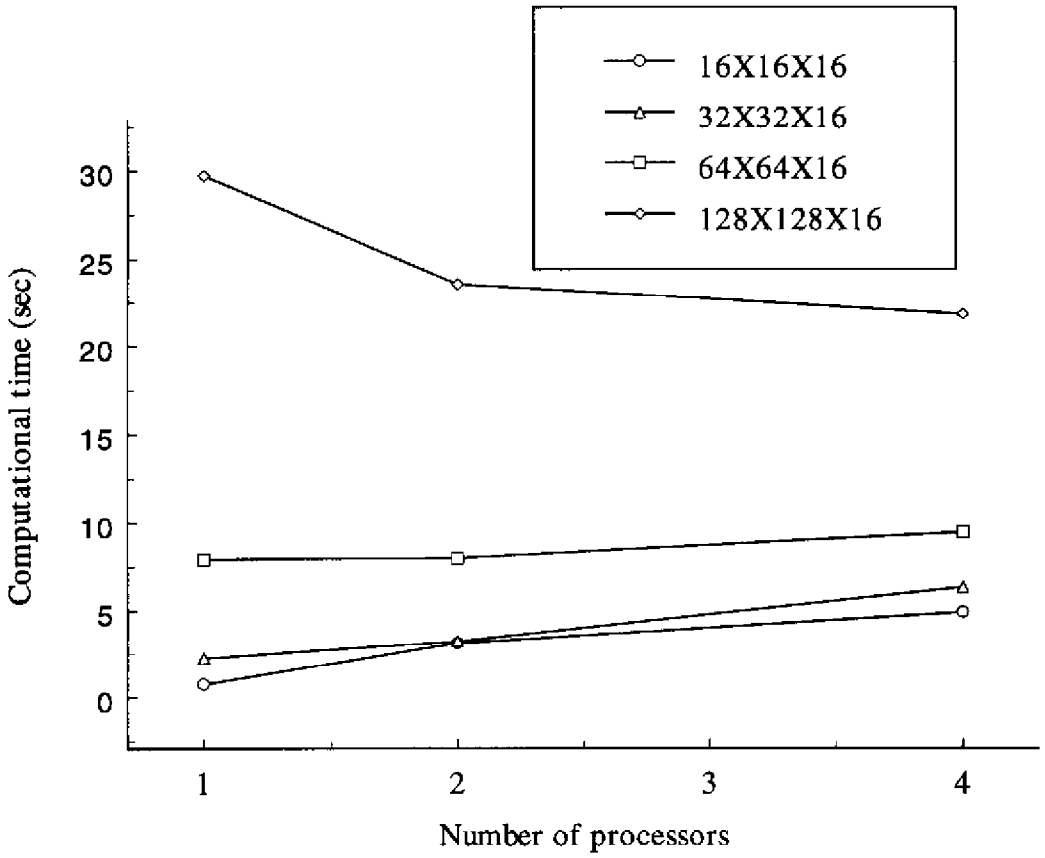

Figure 4.8. Comparison of computational times for solution of fracture pressure equation on the SGI Power Challenge.

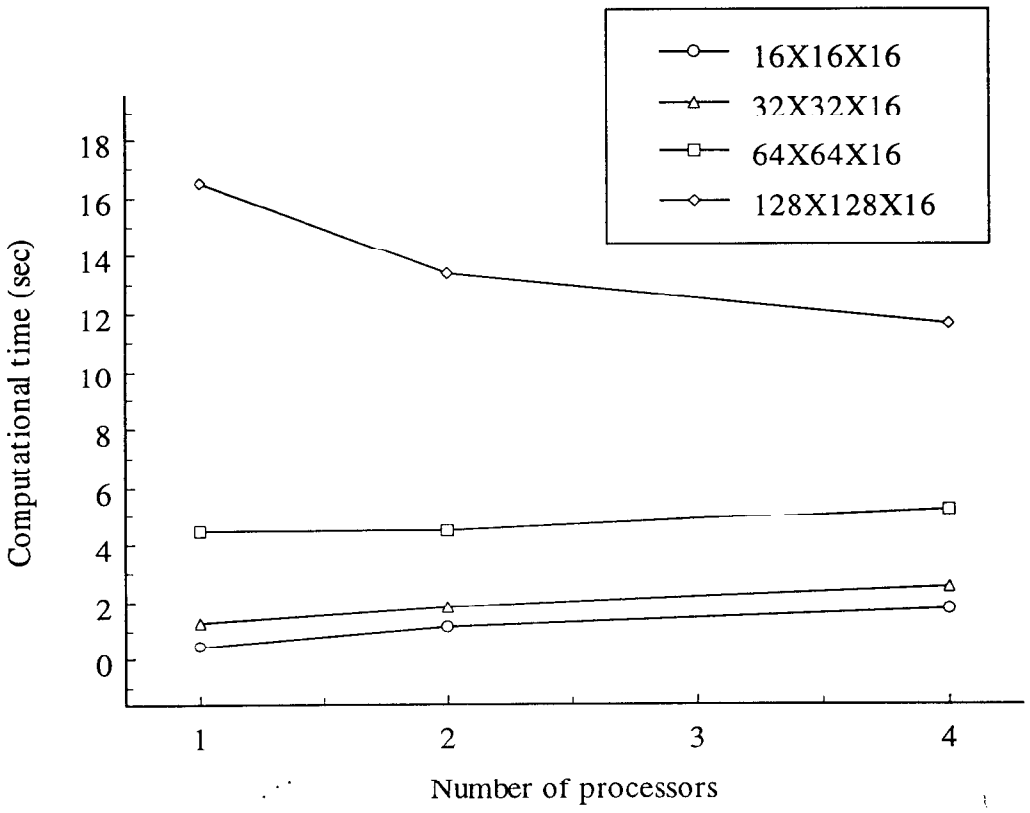

Figure 4.9. Comparison of computation times for the solution of matrix pressure equation on the SGI Power Challenge.

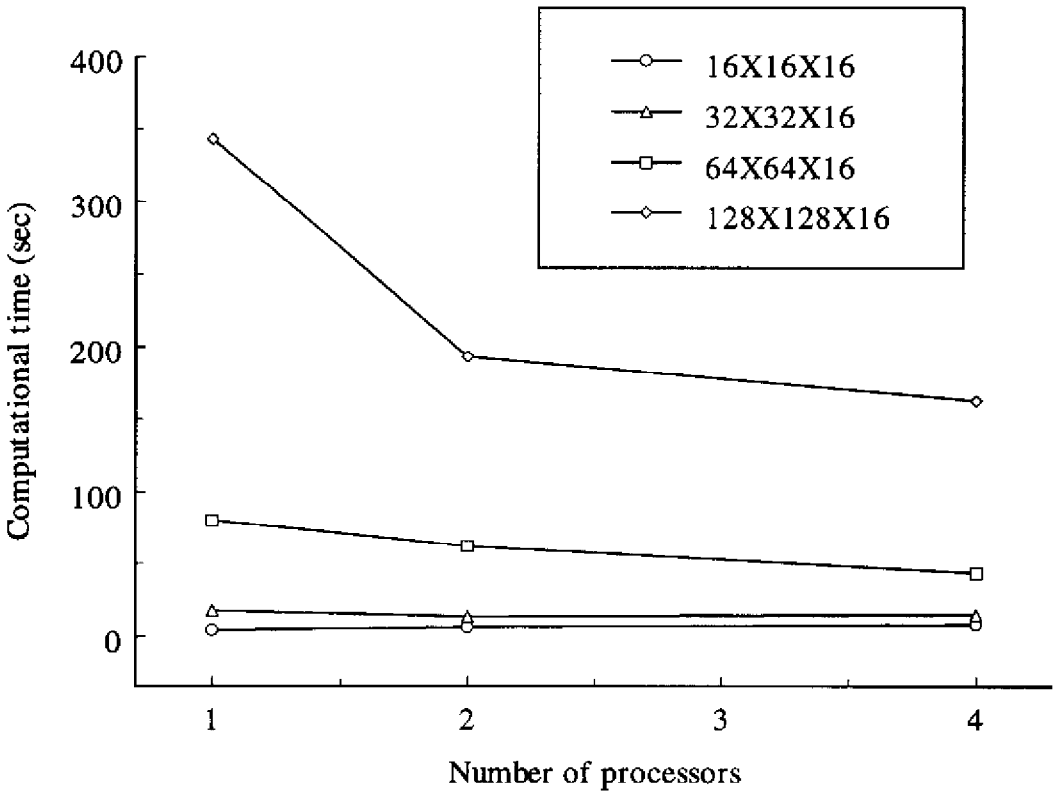

Figure 4.10. Comparison of total computation time for one time step of the simulation on SGI Power Challenge.

5. RECOMPLETION OF THE MICHELLE UTE 7-1 WELL

5.1. Introduction

The recompletion of the Michelle Ute 7-1 well (section 7, T. 1 S., R. 1 E.) was the first step in a three-well demonstration. The Michelle Ute recompletion was designed as a three-stage, high-diversion, high-pressure, acid treatment. Each stage was about a 500-ft (152.5-m) vertical interval with over 10 beds perforated in each interval. The second well demonstration will be a recompletion of the Malnar Pike 1-17A1E well (section 17, T. 1 S., R. 1 E.) which was just beginning as of September 30, 1997. The Malnar Pike recompletion is designed to be an acid treatment at the bed scale, by isolating and treating three or more individual beds. The third well demonstration will be the drilling and completion of a new well. The completion technique used in the new well will be based on the results of the first two recompletions.

As part of the recompletion of the Michelle Ute well the gross productive interval (12,900 to 14,450 ft [3934.5-4407.3 m]) was logged, additional beds were perforated, and the entire interval was stimulated. The operator attempted to stimulate the well at high pressure (about 10,000 psi [68,950 kPa]) at three separate packer locations. But at each location the pressure would not hold. To pull and inspect the tubing would of required several days of rig time and then a possible wait of several more days for the service company scheduled to do the acid treatment to become available again. The operator felt it was more economical to proceed with the acid treatment at lower pressure. The company engineer decided to revert back to the way he had always done it, and pumped the entire job from one packer location rather than go back down hole and pump it at lower pressure, at each of the three locations. The tubing parted when the operator attempted to come out of the hole after the acid treatment, resulting in several days of fishing with the acid left in the hole. As a result, proceeding with the treatment may have been more costly than what the delay would have cost.

The operator swabbed for a week after the fish was retrieved from the hole, then released the work-over rig and continued cleaning up the hole with the downhole pump. The operator intended to run the isotope tracer and anisotropy log through the production tubing after the well was cleaned up but, the anisotropy log was to large to fit through the production packer. The isotope tracer log that was run after the treatment shows that very few of the perforated beds received acid. A comparison of fracture density before and after treatments could not be made since the dipole shear anisotropy log was not run after the treatment as planned. But, the low production rate of the well after the treatment indicates that the low treating pressures probably did not open up any new fractures. The well has produced at an improved rate since the recompletion but far below expectations.

5.2. Cased-Hole Log Interpretation of the Michelle Ute Well

Dipole shear anisotropy (anisotropy) and dual burst thermal decay time (TDT) logs were run before and an isotope tracer log was run after the treatment. The TDT log indicates hydrocarbons in most of the sandstone beds in the logged interval (Figs. 5.1 and 5.2, Log A) as anticipated from analysis of the open-hole logs. The TDT log was used to help select beds to be perforated before the treatment. Perforations are shown in t a comparison of fracture density

before and after treatments could not be he depth column of the TDT log, previous perforations (still open) are on the right, and perforations added with this recompletion are on the left. Some older perforated intervals were re-perforated.

The TDT log was used to qualitatively identify hydrocarbon-bearing beds in the Michelle Ute well. The cross over of the thermal decay porosity and the inelastic counts of the far gate curves were used as a gas indicator. The separation of the total selected counts far detector and near detector curves were used as an oil indicator. All the hydrocarbon-bearing beds identified on the TDT log have indications of both oil and gas, including beds that have never been perforated. Hydrocarbons in this reservoir are single phase (liquid) under original reservoir pressure. Based on the TDT log it appears there is vertical communication in the reservoir causing a reduction in original reservoir pressure in beds that have never been perforated.

The computer-processed log of the anisotropy data (Figs. 5.1 and 5.2, Log B) provides an interpretation of the density of open fractures in the formation before the treatment. The solid black tracings in the depth column of Log B represent the density of open fractures in the formation; the width of the solid black tracing is proportional to the fracture density. The log shows several beds with open fractures (12,990; 13,260 ft [3961.9, 4044.3 m] Fig. 5.1: and 13,500; 13,748; 13846; 13,890 ft [4117.5, 4193.1, 4223.0, 4236.5 m] Fig. 5.2).

The anisotropy log was not run after the treatment as planned so it cannot be determined if new fractures were opened by the treatment. Also, the repeatability of the log (do fractures shown on the first log run show on the second run as well?) is an important aspect of determining the reliability of the data. However, comparison of the dipole sonic to the tracer log does give credence to the fracture interpretation.

The isotope tracer log shows which beds the acid entered by recording the position of encapsulated radioactive isotopes that were added to the acid but remain in the formation after the treatment. The perforations in the upper 500 ft (152.5 m) of the treated interval received most of the acid (Fig. 5.1, Log C). Perforations from 13,400 to 13,550 ft (4087-4133 m) received only a minor amount of acid and from 13,500 ft (4133 m) to total depth, the perforations received no acid (Fig. 5.2, Log C).

The isotope tracer log shows the acid went above or below the perforations in some places, corresponding to fractures indicated on the anisotropy log. Examples of this can be seen from 13,080 to 13,110 ft (3989.4-3998.6 m) and from 13,240-13,250 ft (4038.2-4041.3 m) (Fig. 5.2). Fractures identified in core and borehole imaging logs throughout the Bluebell field typically are highly mineralized. Operators have often speculated that the acid treatments open up these mineralized fractures. The most prominent indication of fractures (12,990: 13,280 ft [3961.9, 4050.4 m] Fig. 5.1: and 13,846 ft [4223.0 m] Fig. 5.2: for example) are in beds that were previously perforated and acidized. Only moderate fracture density is indicated by the anisotropy log in beds that have not been perforated and treated prior to running the log (13,500; 13,520; 13,750 ft [4117.5, 4123.6, 4193.8 m] Fig. 5.2: for example). The prominent fracture at 13,260 ft (4044.3 m) (Fig. 5.1) is an exception.

Core and borehole imaging logs from the Bluebell field show that most fractures terminate at bed boundaries. The bed from 12,985 to 12,996 ft (3960.4-3963.8 m) is separated from the sandstone below by a thin (4-ft [1.2-m]) shale break. The upper bed appears to have fractures that terminate downward at the shale break (Fig. 5.1, Log B) but the lower bed is not fractured. The tracer log shows that acid went into both beds but not the shale break between them (Fig.

5.1, Log C). This indicates that the fractures in the upper bed do terminate at the bed boundary and do not penetrate the shale break.

The vertical communication of the reservoir indicated by the TDT log means there are some extensive, nearly vertical fractures that are not identified in core or logs because they extend beyond the plain of view. Another possibility is individual fracture sets terminate at the bed boundary but sufficient interconnectivity exists between fracture sets to provide vertical communication.

5.3. Acid Treatment of the Michelle Ute Well

The packer and tubing were set at 13,720 ft (4184.6 m) (planned first stage 13,720 to 14,450 ft [4184.6-4407.3 m]) and then at 13,200 ft (4026.0 m) (planned second stage 13,200 to 13,720 ft [4026.0-4184.6 m]). At both locations leakage occurred when the well was pressured tested at 10,000 psi (68,950 kPa). As a result, acid was not pumped at either depth. The packer was set at 12,899 ft (3934.2 m) (planned third stage 12,899 to 13,200 ft [3934.2-4026.0 m]). At 10,000 psi (68,950 kPa) leakage occurred at this depth as well but appeared stable at lower pressures. Therefore, all three stages were pumped over the entire interval (12,899 to 14,450 ft [3934.2-4407.3 m]) from this depth. The treatment (all three stages) consisted of 770 bbl (122,000 L) of total fluid containing 17,500 gallons (66,240 L) of 15% hydrochloric acid, with additives (table 5.1).

Table 5.1. Additives used in the stimulation of the Michelle Ute 7-1 well.

Dowell Commercial Listing	Brief Describtion	Volume Injected
DP104	solvent for solids suspension	155 gallons
FI	scale inhibitor	225 gallons
M275	biocide bacteria control	60 pounds
L55	clay stabilizer	35 gallons
L10	borate cross linking agent	12 pounds
J66	rock salt, diverting agent	3,250 pounds
J227	benzoic acid flakes, diverting agent	3,250 pounds
J424	powdered guar gum polymer	350 gallons
A261	corrosion inhibitor	88 gallons
W54	non-emulsifier	55 gallons
M2	base for pH control	10 pounds
L62	iron stabilizer	253 pounds
L401	iron stabilizer	175 gallons
Radioactive isotopes	antimony and iridium	

The treatment was pumped at a maximum pressure of 6500 psi (44,820 kPa), an average pressure of 5500 psi (37,920 kPa), a maximum rate of 12.8 bbl/min (2000 L/min), and an average rate of 11.1 bbl/min (1800 L/min). The initial shut-in pressure was 4500 psi (31,030 kPa). After 5 minutes the shut-in pressure was 2125 psi (14,650 kPa). The well was opened and about 30 bbl (5,000 L) of fluid flowed back. The high-pressure tubing needed for the treatment parted when the operator attempted to pull out of the hole. As a result most of the acid remained in the hole for several days until the test string could be retrieved and replaced with the production packer and tubing.

5.4. Oil Production Before and After Stimulation

The Michelle Ute 7-1 well was completed in April 1984 flowing 451 BO (63.1 MT) and 240 thousand cubic feet of gas (MCFG [6.79 m^3]) per day. The cumulative production as of December 31, 1996, before the demonstration was 118,408 BO (16,577.1 MT) and 99,009 MCFG (2803.93 m^3) (Fig. 5.3).

The Michelle Ute well produced an average of 19 BO per day (2.7 MT) prior to the acid treatment (Fig. 5.3). The well was shut in on a regular basis as the daily rate dropped below economic limits. After the treatment, the well produced about 40 BO (5.6 MT) per day initially, but production rapidly declined to near the previous rate. In June 1997, based on additional swab testing, the location of the down-hole pump was moved uphole to increase efficiency (less hydrostatic pressure on the formation), resulting in an increase in daily oil production. The rate has remained fairly consistent since moving the pump. The increased production is encouraging considering how few beds were actually treated. The increased production is probably due to the acid cleaning up scale and paraffin buildup around the perforations and near wellbore area.

5.5. Summary and Conclusions

The recompletion of the Michelle Ute 7-1 well was not a valid demonstration of a high-pressure, high-diversion, staged completion technique because of mechanical problems during the treatment. The operator decided to treat the entire 1550-ft (472.8-m) interval from one packer location instead of three separate intervals of about 500-ft (152.5-m) each. The isotope tracer log shows that only perforated beds in the first 500 ft (152.5-m) below the packer received any acid. The improvement in the production rate is encouraging considering the lower than normal treating pressures and that few of the beds were actually treated.

The dual burst thermal decay time and dipole shear anisotropy logs appear to be reliable tools for evaluating remaining hydrocarbon potential and fracture density in a cased-hole well that has been producing oil for many years. This type of data can be used to identify potentially productive beds that are not perforated in older wells, eliminate the acidizing of previously perforated beds that have little to no potential, and determine if the acid fracture treatment is hydraulically fracturing the formation.

Figure 5.1. Cased-hole logs (13,400-13,900 ft [4,073.6-4,225.6 m]) of a portion of the Flagstaff Member of the Green River Formation in the Michelle Ute 7-1 well. Log A is the dual burst thermal decay time log; Log B is a portion of the dipole shear anisotropy log; and Log C is the isotope tracer log. See the text for detailed explanation and interpretation of the logs.

Figure 5.2. Cased-hole logs (12,900-13,400 ft [3,921.6-4,073.6 m]) of a portion of the Flagstaff Member of the Green River Formation in the Michelle Ute 7-1 well. Log A is the dual burst thermal decay time log; Log B is a portion of the dipole shear anisotropy log; and Log C is the isotope tracer log. See the text for detailed explanation and interpretation of the logs.

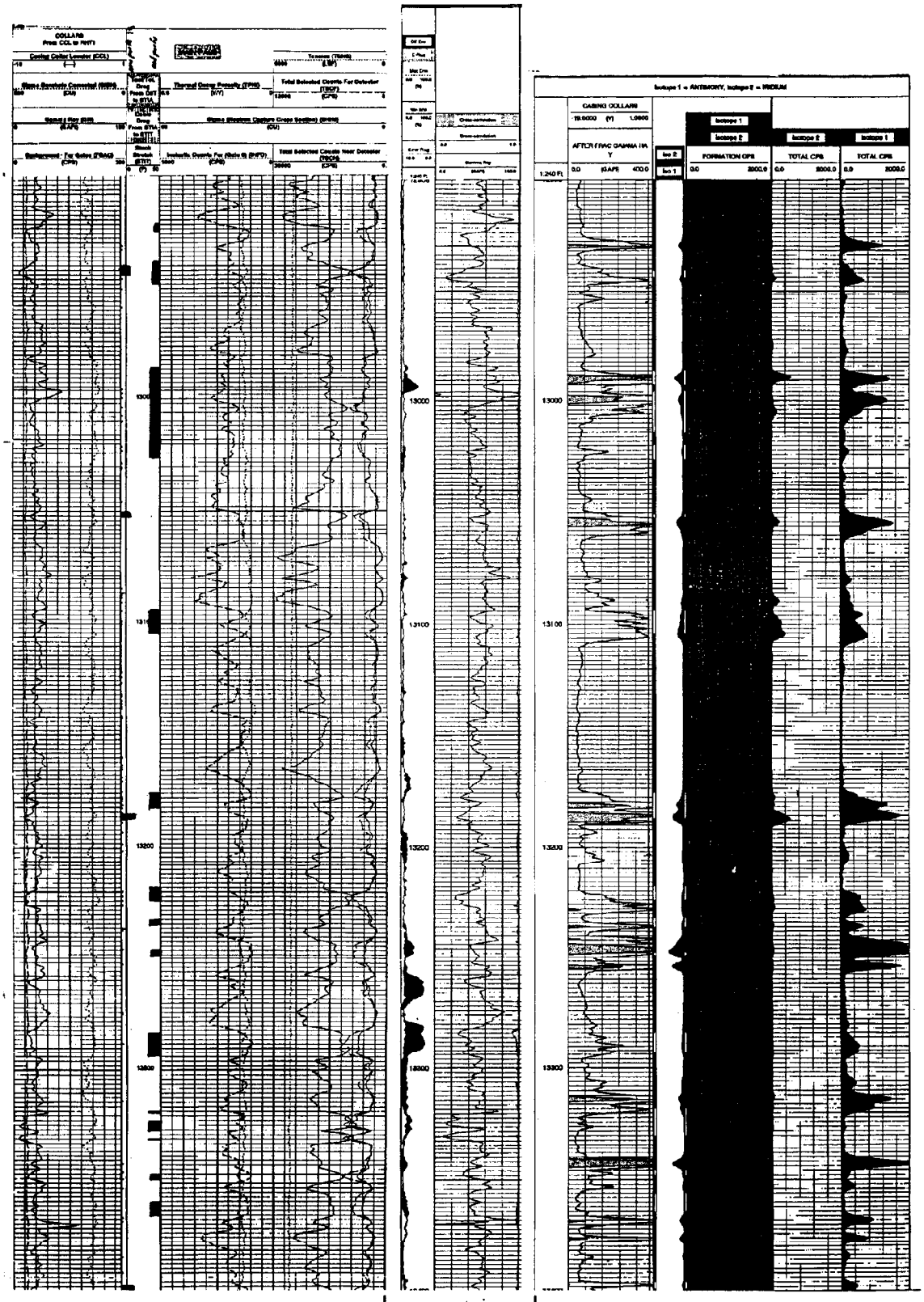

Log A | Log B | Log C

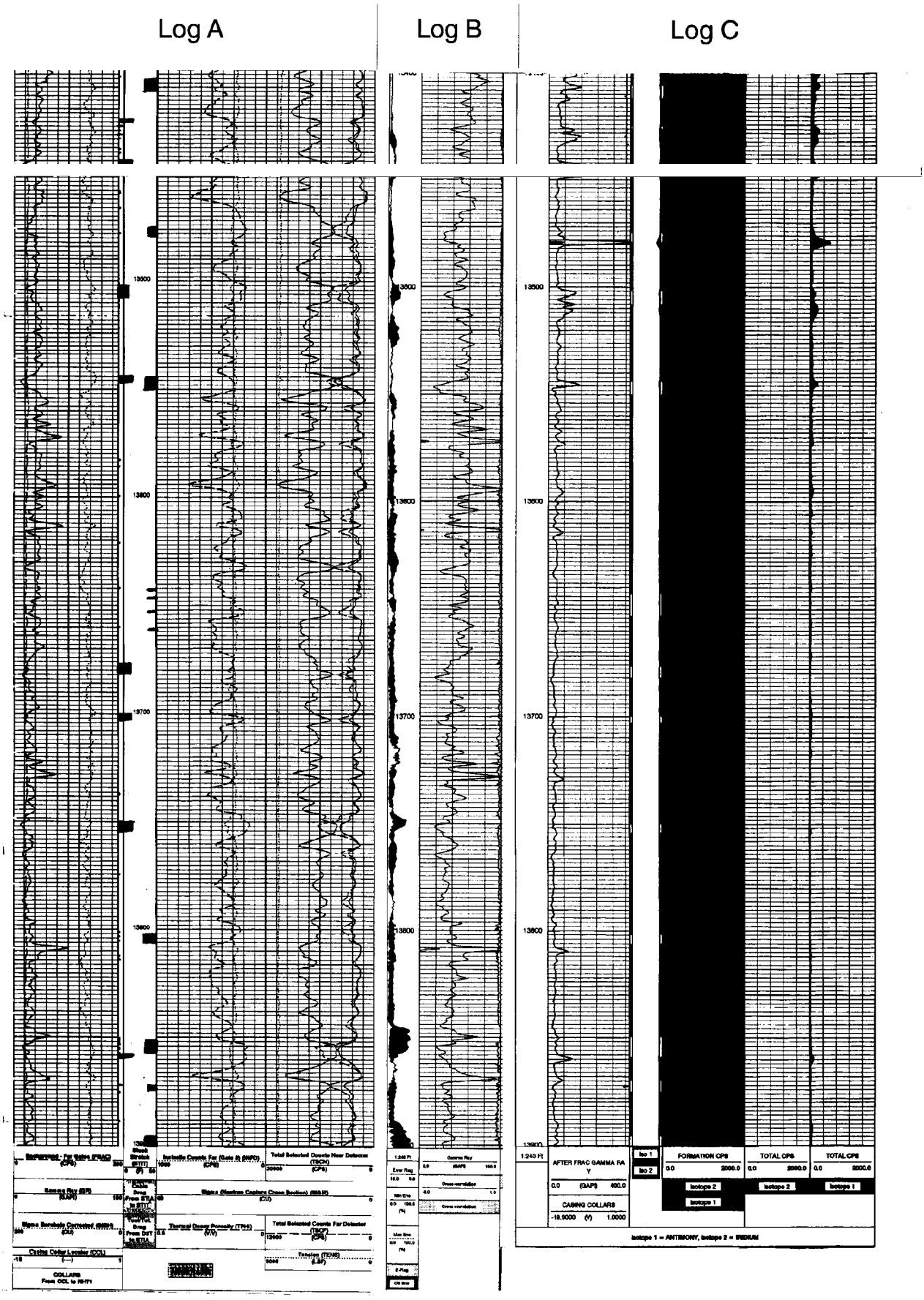
Log A
Log B
Log C
13500
13600
13700
13800
1240 Ft
AFTER FRAG GAMMA RA
CASING COLLARS
FORMATION CPS
TOTAL CPS
TOTAL CPS
Isotope 1 = ANTIMONY, Isotope 2 = IRIDIUM

Fig 5.2

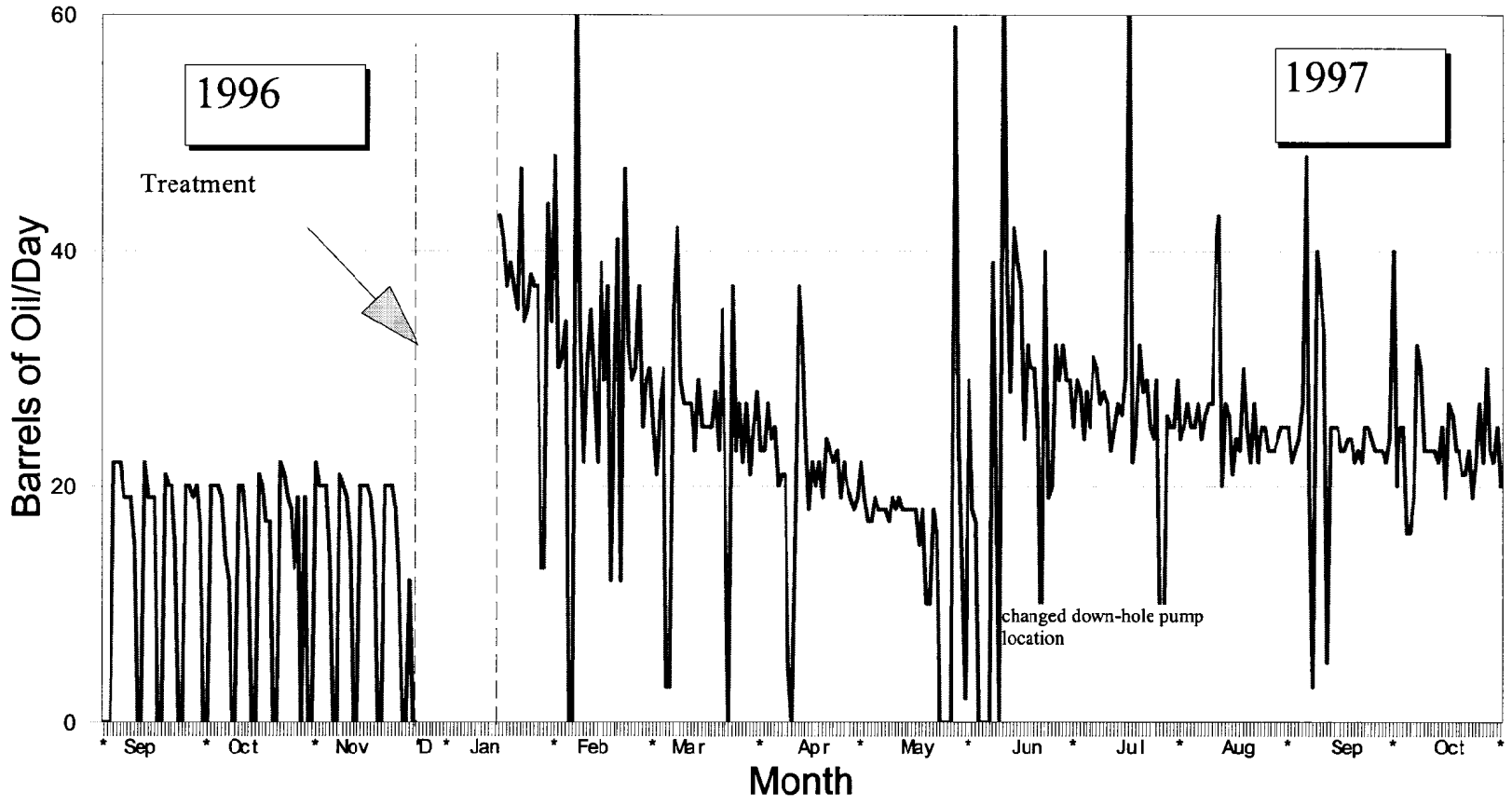

Figure 5.3. Daily oil production from the Michelle Ute 7-1 well three months before and 10 months after the acid treatment.

6. TECHNOLOGY TRANSFER

6.1. Introduction

Technology transfer activities for the year highlighting the demonstration activities of the project include information exhibits at one regional and one national petroleum industry meeting, one published abstract, and poster display at the national meeting. Articles were published in the Utah Geological Survey *Petroleum News* and *Survey Notes* while daily activity reports for the first demonstration were posted on the Bluebell project home page.

6.2. Information Exhibits

American Association of Petroleum Geologists, Annual Meeting and Exhibition, April 1997, Dallas, TX.

American Association of Petroleum Geologists, Rocky Mountain Section Meeting, August 1997, Denver, CO.

6.3. Publications

Morgan, C.D., 1997, *Improving primary oil recovery from a (DOE Class I) fluvial-dominated deltaic lacustrine reservoir Uinta Basin, Utah*: American Association of Petroleum Geologists Official Program, p. A85.

Utah Geological Survey, 1997, *Oil recovery demonstration program begins with acid treatment in the Bluebell field*: Survey Notes, v. 29, no. 3, p. 10.

6.4. Petroleum News

Petroleum News is a newsletter published semi-annually by the Utah Geological Survey. The newsletter keeps petroleum companies, researchers, and other parties involved in exploring and developing Utah's' energy resources informed of the progress on various energy-related projects of the Utah Geological Survey. The newsletter is free to anyone interested and is currently sent to roughly 750 individuals and organizations. The most recent issue was published April 1997 for distribution at the Annual Meeting of the American Association of Petroleum Geologists.

6.5. Internet

The Utah Geological Survey maintains a Bluebell home page on its web site containing the following information: (1) a description of the project, (2) a list of project participants, (3) each of the Quarterly Technical Progress Reports, (4) a description of planned field demonstration work, (5) portions of the Annual Technical Reports with information on where to obtain complete reports, (6) a reference list of all publications that are a direct result of the project, (7) an

extensive selected reference list for the Uinta Basin and lacustrine deposits worldwide, and (8) daily activity reports of the Michelle Ute 7-1 and the Malnar Pike 17-1 demonstration work. The home page address is: *http://www.ugs.state.ut.us/bluebell.htm*

REFERENCES

Allison, M.L., 1996, Increased oil production and reserves from improved completion techniques in the Bluebell field, Uinta Basin, Annual Report for the period October 1, 1993 to September 30, 1994: U.S. National Technical Information Service DE95000171, 123 p.

Allison, M.L., and Morgan, C.D., 1996, Fracture analyses, *in* Allison, M.L., and Morgan, C.D., editors, Increased oil production and reserves from improved completion techniques in the Bluebell field, Uinta Basin, Annual Report for the period October 1, 1994 to September 30, 1995: U.S. National Technical Information Service DE96001227, p. 48-51.

Bredehoeft, J.D., Wesley, J.B., and Fouch, T.D., 1994, Simulation of the origin of fluid pressure, fracture generation, and the movement of fluids in the Uinta Basin, Utah: American Association of Petroleum Geologists Bulletin, v. 78, no. 11, p. 1729-1747.

Castle, J.W., 1991, Sedimentation in Eocene Lake Uinta (lower Green River Formation), northeastern Uinta Basin, Utah, *in* Katz, B.J., editor, Lacustrine basin exploration-case studies and modern analogs: American Association of Petroleum Geologists Memoir 50, p. 243-263.

Curtice, Richard, 1996, Completion techniques, *in* Allison, M.L., and Morgan, C.D., editors, Increased oil production and reserves from improved completion techniques in the Bluebell field, Uinta Basin, Annual Report for the period October 1, 1994 to September 30, 1995: U.S. National Technical Information Service DE96001227, p. 77-92.

Deutsch, C.V., and Journel, A.G., 1992, Geostatistical software library and users' guide: New York, Oxford University Press.

Fouch, T.D., 1975, Lithofacies and related hydrocarbon accumulations in Tertiary strata of the western and central Uinta Basin, Utah, *in* Bolyard, D.W., editor, Symposium on deep drilling frontiers in the central Rocky Mountains: Rocky Mountain Association of Geologists Special Publication, p. 163-173.

---1976, Revision of the lower part of the Tertiary system in the central and western Uinta Basin, Utah: U.S. Geological Survey Bulletin 1405-C, 7 p.

---1981, Distribution of rock types, lithologic groups, and interpreted depositional environments for some lower Tertiary and Upper Cretaceous rocks from outcrops at Willow Creek - Indian Canyon through the subsurface of Duchesne and Altamont oil fields, southwest to north-central parts of the Uinta Basin, Utah: U.S. Geological Survey Oil and Gas Investigations Map, Chart OC-81, 2 sheets.

Fouch, T.D., and Pitman, J.K., 1991, Tectonic and climate changes expressed as sedimentary cycles and stratigraphic sequences in the Paleogene Lake Uinta system, central Rocky Mountains, Utah and Colorado: American Association of Petroleum Geologists Bulletin, v. 75, no. 3, p. 575.

---1992, Tectonic and climate changes expressed as sedimentary and geochemical cycles - Paleogene Lake systems, Utah and Colorado - implications for petroleum source and reservoir rocks, *in* Carter, L.J., editor, U.S. Geological Survey Research on Energy Resources, 1992 McKelvey Forum Program and Abstracts: U.S. Geological Survey Circular 1074, p. 29-30.

Fouch, T.D., Pitman, J.K., Wesley, J.B., Szantay, Adam, and Ethridge, F.G., 1990, Sedimentology, diagenesis, and reservoir character of Paleogene fluvial and lacustrine rocks, Uinta Basin, Utah - evidence from the Altamont and Red Wash fields, *in* Carter, L.M., editor, Sixth V. E. McKelvey forum on mineral and energy resources, U.S. Geological Survey Research on Energy Resources - 1990 - Program and Abstracts: U.S. Geological Survey Circular 1060, p. 31-32.

Franczyk, K.J., Fouch, T.D., Johnson, R.C., Molenaar, C.M., and Cobban, W.A., 1992, Cretaceous and Tertiary paleogeographic reconstructions for the Uinta-Piceance Basin study area, Colorado and Utah: U.S. Geological Survey Bulletin 1787-Q, 37 p.

Hofhaus, J. and Van de Velde, E. F., 1995, Alternating direction line-relaxation methods on multicomputers, SIAM (Society of Industrial and Applied Mathematics) Journal of Science and Computing, vol. 17, No. 2, p. 454-478.

Lucas, P.T., and Drexler, J.M., 1975, Altamont-Bluebell - a major fractured and overpressured stratigraphic trap, Uinta Basin, Utah *in* Bolyard, D.W., editor, Symposium on deep drilling frontiers of the central Rocky Mountains: Rocky Mountain Association of Geologists, p. 265-273.

Morgan, C.D., 1997, Subsurface mapping and well log analysis, *in* Morgan, C.D., editor, Increased oil production and reserves from improved completion techniques in the Bluebell field, Uinta Basin, Utah, Annual Report for the period October 1, 1995 to September 30, 1996: U.S. National Technical Information Service DE96001297, p. A1-A49.

Osmond, J.C., 1964, Tectonic history of the Uinta Basin, Utah, *in* Sabatka, E.F., editor, Guidebook to the geology and mineral resources of the Uinta Basin: Intermountain Association of Petroleum Geologists Thirteenth Annual Field Conference, p. 46-58.

Pitman, J.K., Fouch, T.D., and Goldhaber, M.B., 1982, Depositional setting and diagenetic evolution of some Tertiary unconventional reservoir rocks, Uinta Basin, Utah: American Association of Petroleum Geologists Bulletin, v. 66, no. 10, p. 1581-1596.

Ryder, R.T., Fouch, T.D., and Elison, J.H., 1976, Early Tertiary sedimentation in the western Uinta Basin, Utah: Geological Society of America Bulletin, v. 87, p. 496-512.

Stokes, W.L., 1986, Geology of Utah: Utah Geological Survey Special Publication no. 6, 280 p.

Wegner, Marybeth, 1996, Core analysis and description as an aid to hydrocarbon production enhancement - Lower Green River and Wasatch Formations, Bluebell field, Uinta Basin, Utah: Provo, Brigham Young University, M. S. Thesis, Department of Geology, 233 p.

Wegner, MaryBeth, and Morris, T.H., 1996, Core analyses of the lower Green River and Wasatch Formations, *in* Allison, M.L., and Morgan, C.D., editors, Increased oil production and reserves from improved completion techniques in the Bluebell field, Uinta Basin, Utah, Annual report for the period October 1, 1994 to September 30, 1995: U.S. National Technical Information Service DE96001227, p. 35-47.